AD-A065 180 SOUTHWEST RESEARCH INST SAN ANTONIO TEX F/G 11/6
RESEARCH ON GROWTH OF MICROCRACKS IN NICKEL-BASE SUPERALLOYS.(U)
SEP 78 T S COOK, J LANKFORD, G P SHELDON F33615-76-C-5242
UNCLASSIFIED SWRI-02-4601 AFML-TR-78-133 NL

1 OF 2
ADA
065180

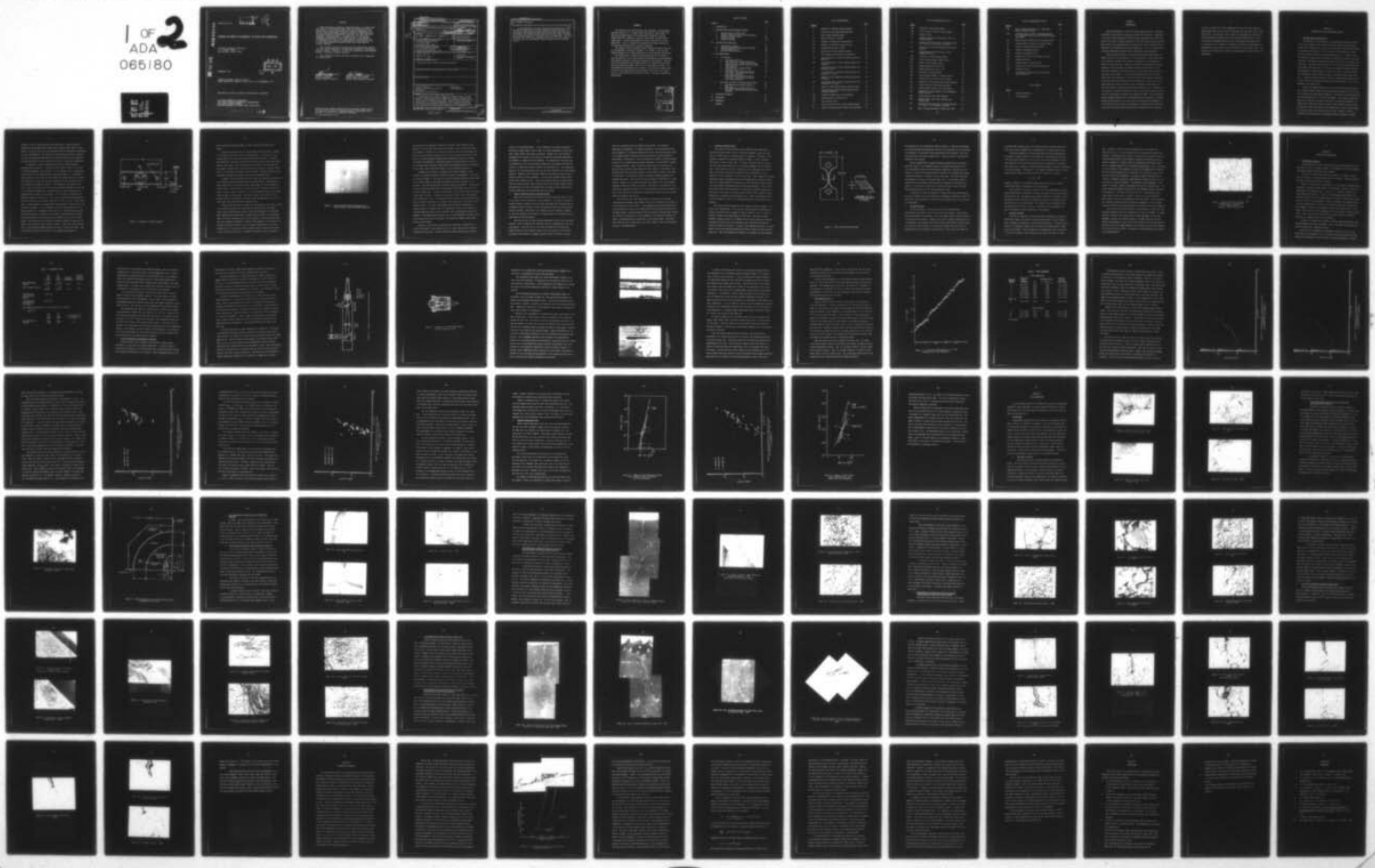

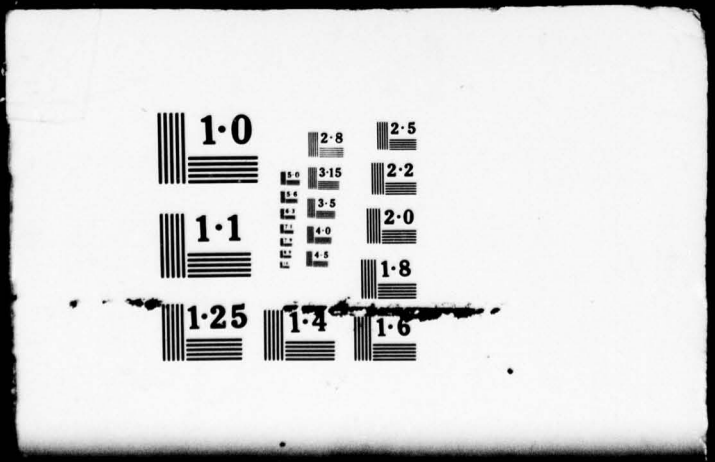

AFML-TR-78-133

LEVEL II

12 SC

RESEARCH ON GROWTH OF MICROCRACKS IN NICKEL-BASE SUPERALLOYS

Southwest Research Institute
P. O. Drawer 28510
San Antonio, Texas 78284

DECEMBER 1978

TECHNICAL REPORT AFML-TR-78-133
FINAL REPORT FOR PERIOD 1 JUNE 1976 to 30 SEPTEMBER 1978

Approved for public release; distribution unlimited

AIR FORCE MATERIALS LABORATORY
AIR FORCE WRIGHT AERONAUTICAL LABORATORIES
AIR FORCE SYSTEMS COMMAND
WRIGHT-PATTERSON AIR FORCE BASE, OHIO 45433

NOTICE

When Government drawings, specifications, or other data are used for any purpose other than in connection with a definitely related Government procurement operation, the United States Government thereby incurs no responsibility nor any obligation whatsoever; and the fact that the said drawings, specifications, or other data, is not to be regarded by implication or otherwise as in any manner licensing the holder or any other person or corporation, or conveying any rights or permission to manufacture, use, or sell any patented invention that may in any way be related thereto.

This report has been reviewed by the Information Office (IO) and is releasable to the National Technical Information Service (NTIS). At NTIS, it will be available to the general public, including foreign nations.

This technical report has been reviewed and is approved for publication.

WALTER H. REIMANN
Project Engineer
Metals Behavior Branch

NATHAN G. TUPPER, Chief
Metals Behavior Branch
Metals and Ceramics Division

Copies of this report should not be returned unless return is required by security considerations, contractual obligations, or notice on a specific document.

AIR FORCE/56780/16 February 1979 — 400

UNCLASSIFIED

SECURITY CLASSIFICATION OF THIS PAGE *(When Data Entered)*

REPORT DOCUMENTATION PAGE

READ INSTRUCTIONS BEFORE COMPLETING FORM

1. REPORT NUMBER: AFML-TR-78-133	2. GOVT ACCESSION NO.
3. RECIPIENT'S CATALOG NUMBER	
4. TITLE (and Subtitle): Research on Growth of Microcracks in Nickel-Base Superalloys	5. TYPE OF REPORT & PERIOD COVERED: Final Report, July 1976 - July 1978
6. PERFORMING ORG. REPORT NUMBER: SWRI-02-4601	
7. AUTHOR(s): T. S. Cook, J. Lankford, G. P. Sheldon	8. CONTRACT OR GRANT NUMBER(s): F33615-76-C-5242
9. PERFORMING ORGANIZATION NAME AND ADDRESS: Southwest Research Institute, P. O. Drawer 28510, San Antonio, Texas 78284	10. PROGRAM ELEMENT, PROJECT, TASK AREA & WORK UNIT NUMBERS
11. CONTROLLING OFFICE NAME AND ADDRESS: Air Force Materials Laboratory, Air Force Systems Command, Wright-Patterson AFB, Ohio 45433	12. REPORT DATE: September 1978 13. NUMBER OF PAGES: 93 + prelims
14. MONITORING AGENCY NAME & ADDRESS *(if different from Controlling Office)*: 103p.	15. SECURITY CLASS. *(of this report)*: UNCLASSIFIED 15a. DECLASSIFICATION/DOWNGRADING SCHEDULE

16. DISTRIBUTION STATEMENT *(of this Report)*

Approved for public release; distribution unlimited.

17. DISTRIBUTION STATEMENT *(of the abstract entered in Block 20, if different from Report)*

18. SUPPLEMENTARY NOTES

19. KEY WORDS *(Continue on reverse side if necessary and identify by block number)*

Fracture Mechanics
Fatigue of Nickel-Base Superalloys
Microcracks
Scanning Electron Microscope
Fractography
Crack Initiation

20. ABSTRACT *(Continue on reverse side if necessary and identify by block number)*

The growth of very small, 0.06-0.15 mm, fatigue cracks in a powder metallurgy nickel-base superalloy, IN-100, was studied. Tests were conducted at room temperature and at 650°C. The crack growth rates were measured by means of a 600X microscope which allowed in situ crack length measurement, even at elevated temperature. The interaction of the crack and the material microstructure was observed in a fatigue loading stage which operated in the Scanning Electron Microscope. A technique for

over

DD FORM 1 JAN 73 1473 EDITION OF 1 NOV 65 IS OBSOLETE

UNCLASSIFIED

SECURITY CLASSIFICATION OF THIS PAGE *(When Data Entered)*

328200

20. ABSTRACT (Continued)

experimentally determining stress intensity factors was also developed.

At room temperature, the small fatigue cracks propagated more rapidly than would be predicted by data from conventional fatigue specimens. As the stress intensity level increased, the long and short crack growth rate data merged. This behavior was not observed at elevated temperature where the long and short crack data agreed over the entire test range. One 650°C short crack was subjected to a one minute dwell at maximum load. This crack propagated more slowly than a comparable long crack. This effect appears to be the result of time dependent inelastic deformation at the specimen surface.

FOREWORD

The research study reported herein was conducted at the Southwest Research Institute, P. O. Drawer 28510, San Antonio, Texas 78284. The work was performed under Air Force Materials Laboratory, Contract F33615-76-C-5242, "Research on Growth of Microcracks in Nickel-Base Superalloys". Period of performance was from 1 June 1976 to 30 September 1978. Dr. W. H. Reimann of the Metals and Ceramics Division of the Materials Laboratory was the project engineer.

The research work was performed within Southwest Research Institute by the Department of Materials Sciences. Dr. Thomas S. Cook was the program manager and Dr. James Lankford was the co-principal investigator.

The authors wish to express their appreciation for the careful work and expertise of Mr. Harold Saldana in developing the metallographic and specimen preparation techniques required by this program. The dedication and innovative skills demonstrated by Mr. Richard Atiyeh during the crack growth experiments were a key to the program's success. The interferometric measurements of the plastic zone size by Dr. Wayne Jones of the Air Force Materials Laboratory played a key role in the verification of the specimen stress intensity factor. His help is gratefully acknowledged.

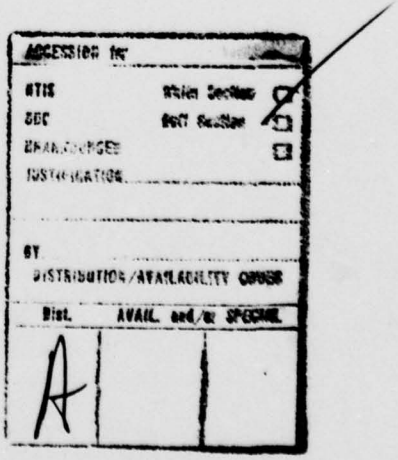

TABLE OF CONTENTS

SECTION			Page
I	INTRODUCTION		1
II	SPECIMEN DESIGN AND PRELIMINARY STUDIES		3
	1.	Specimen Design Considerations	3
	2.	Impact of Material Voids on Specimen Design	9
	3.	Alternate Specimen Design	11
	4.	Specimen Analysis	13
	5.	Etching of IN-100	14
III	FATIGUE CRACK GROWTH DATA		17
	1.	Experimental Technique	17
	2.	Elevated Temperature Experimental Technique	19
	3.	Room Temperature Data	26
	4.	Elevated Temperature Data	37
IV	SEM OBSERVATIONS		42
	1.	Fractography	42
		a. LCF Tests of IN-100	42
		b. Room Temperature Fatigue Fracture of Center Hole Razor Blade IN-100 Specimen	45
		c. Room Temperature Fatigue Fracture of DEN IN-100 Specimen	48
		d. Room Temperature Bending Fatigue Fracture of Rene´ 95	48
		e. Room Temperature Fatigue Fracture of Precracked, Reduced-Section IN-100 Razor Blade Specimens	51
		f. High Temperature Fatigue Fracture of Precracked, Reduced-Section IN-100 Razor Blade Specimens	55
	2.	Crack Path and Crack Tip Opening Observations	59
		a. Room Temperature Fatigue Fracture of Rene´ 95	64
		b. Room Temperature Fatigue Fracture of Precracked, Reduced-Section Razor Blade Specimens	64
V	DISCUSSION OF RESULTS		77
VI	CONCLUSIONS		85
VII	REFERENCES		87
	APPENDIX		

LIST OF ILLUSTRATIONS

Figure		Page
1	Schematic of Original Fatigue Specimen	5
2	Surface Void Near Edge Containing Crack	7
3	Final Fatigue Specimen Design	12
4	Typical Structure of IN-100	16
5a	Schematic of High Resolution Microscope	21
5b	Schematic of Reflective Objective Lens	22
6a	Completed Microscope in Place	24
6b	Specimen and Fixtures Mounted in Oven	24
7	Crack Length vs Cycles Plot for Specimen 2	27
8a	Crack Growth Rate vs Stress Intensity Factor for Specimen 2	30
8b	Crack Growth Rate vs Stress Intensity Factor for Specimen 2	31
9	Crack Growth Rate vs Stress Intensity Factor for Specimens 6 and 7	33
10	Crack Growth Rate vs Stress Intensity Factor for Specimens 3, 4, and 5	35
11	Summary of Room Temperature Fatigue Crack Growth Rate Data	38
12	Crack Growth Rate vs Stress Intensity Factor for Specimens 9, 10, and 11	39
13	Summary of 650°C Fatigue Crack Growth Rate Data	40
14	Initiation Site in LCF Specimen Resulting from Unsintered Material	43
15a	Thumbnail Fatigue Crack in LCF Specimen	43
15b	Voids Located at Initiation Site	44
15c	Close View of Voids	44
16	Void at Initiation Site of Razor Blade Specimen	46
17	Sketch of Failure Surface of Razor Blade Specimen	47

LIST OF ILLUSTRATIONS (Cont'd)

Figure		Page
18a	Macroview of DEN Fatigue Surface	49
18b	Void at Origin of Failure in DEN Specimen	49
18c	Closeup of Void	50
19	Carbide Located at the Taper Edge of Rene´ 95 Bending Specimen	50
20	Initial Crack Found in Rene´ 95 Bending Specimen No. 3 After 3.0×10^6 Cycles, Left Side	52
21	Fracture Surface of Room Temperature Microcrack Specimen	53
22a	Crystallographic Fatigue Surface of Room Temperature IN-100	54
22b	Striations on IN-100 Fatigue Surface	54
23a	Etched Crystallographic Fatigue Surface	56
23b	Etched Striated Fatigue Surface	56
23c	Higher Magnification View of 23a	57
23d	Higher Magnification View of 23b	57
24a	Striations on Fatigue Surface	58
24b	Crystallographic Region at Specimen Surface	58
25a	Fracture Surface of 650°C Cyclic Specimen	60
25b	Comparison of Precrack and 650°C Fatigue Specimen	60
26	Fracture Surface of 650°C Dwell Specimen	61
27a	Crystallographic Surface in Precrack Region	62
27b	Comparison of Crystallographic and Intergranular Fatigue Surfaces	62
28a	Fatigue Surface, 650°C Dwell Specimen	63
28b	Fatigue Surface, 650°C Dwell Specimen Near Specimen Edge	63
29a	Initial Crack Found in Rene´ 95 Bending Specimen No. 2 After 1.3×10^6 Cycles, Left Side	65
29b	Rene' 95 Bending Specimen #2, Right Side. 645X	66

LIST OF ILLUSTRATIONS (Cont'd)

Figure		Page
30a	Rene´ 95 Bending Specimen No. 2, Right Side, Crack Tip and Slip Lines	67
30b	Closeup of Region in Rene´ 95 Bending Specimen No. 2 Showing Fracture Surface and Crack Crossing Slip Region	68
31a	Fatigue Crack in IN-100 Prior to Cycling in SEM	70
31b	Fatigue Crack in Tip Prior to Cycling in SEM	70
32	Crack Tip During Cycling in the SEM	71
33a	Closeup of Unloaded Crack Tip	72
33b	Closeup of Loaded Crack Tip	72
34a	Loaded Crack Tip for Crack Length of 0.5 mm	73
34b	Unloaded Crack Tip	73
35	Cracking Ahead of Main Crack Tip	74
36a	Loaded Crack Tip and Associated Microcrack	75
36b	Unloaded Crack Tip	75
37	Correspondence Between Fracture Surface and Crack Growth Rate	79

LIST OF TABLES

Table		Page
1	Material Properties	18
2	Test Parameters	28

SECTION I

INTRODUCTION

Improved performance of aircraft turbine engines provides a continuous requirement for materials of increased strength and reliability. Responding to the need, powder metallurgy (PM) nickel-base superalloys have been incorporated into disks in engines developed for the F15 and F16 military aircraft. These alloys offer improved specific strength and low cycle fatigue lives in comparison to conventionally processed superalloys. Also, the refined microstructure substantially enhances their inspectability by ultrasonics.

Current design systems for conventionally processed disks define the number of cycles to the formation of a 0.8 mm (0.030 in.) long surface crack as "initiation" lifetime; this lifetime corresponds to the propagation or linkup of microcracks over a distance equivalent to approximately 10 grains. Subsurface crack initiation in wrought nickel-base alloy disks has been virtually nonexistent, and surface cracks of this length have been readily detectable by wink Zyglo. In the powder metallurgy superalloys, however, there exists the possibility of crack initiation from subsurface nonmetallic inclusions, imperfectly sintered particle boundaries, or voids left by the powder metallurgy process; moreover, the conventional "initiation" crack size may represent a dangerously high crack propagation rate. Therefore, it is necessary to relate the lifetime of disks to the initial flaw size distribution as determined by nondestructive examination (NDE). This requirement places stringent demands upon the reproducibility and resolution of the NDE methods and procedures; at the same time the cleanliness and homogeneity of the PM alloys not only reduce the uncertainty of inspection but enhance the resolution of the NDE, allowing much smaller imperfections to be detected.

In order to predict the crack propagation life from very small flaws, the design system must be able to deal confidently with the growth rates of very small flaws. The new alloys thus require the development and evaluation of fracture mechanics methodology for flaw sizes and growth rates on a scale on an order of magnitude below that for conventionally processed alloys. In particular, it is necessary to determine the limits of applicability of deterministic linear elastic fracture mechanics for very small cracks. The objective of this work was to make this determination for small flaws in PM superalloys.

SECTION II

SPECIMEN DESIGN AND PRELIMINARY STUDIES

1. Specimen Design Considerations

The objective of the program was to quantitatively study the growth of very fine fatigue cracks in powder metallurgy (PM) nickel-base superalloys and to determine the extent of the interaction between the crack and the material microstructure. For the purpose of this program, the term "crack" was meant to apply in an engineering sense, i.e., a Mode I crack. The intention, however, was to locate and observe these cracks as soon after initiation as possible, preferably when they were still of the order of the grain size. Since the alloy selected for this study, Gatorized IN-100, has an extremely fine grain size, 3-5 microns, the program objectives required the measurement of small changes in very small cracks. Precisely because these behavioral features might be masked by specimen design, preparation, etc., a concerted effort was made to develop a specimen which would be free of such secondary influences and would allow the measurement of the "true" behavior of the small crack.

Because the specimen designed for this program was unique and because the original specimen design was changed during the program, it will be useful to present some background information on the design of the specimen and the material behavior as it affected the design. The original concept was based on the idea that the small crack had to be naturally initiated; anything which artificially aided the fatigue crack initiation process could, in this view, alter the results in some unknown way. Based on this premise, no notches or other crack starters could be used. However, in order to localize the initiation area, the specimen would be fatigued in bending;

moreover, to aid in initiation and crack resolution, a tapered edge was polished on the specimen, since cracks tend to form at sharp edges in superalloys. Of course, since the stress gradient makes the bending test unsuitable for crack propagation, it was planned to only initiate the crack in bending. Once the tiny crack had been identified, the load frame would be changed and the specimen would be cycled in tension during the crack growth measurements.

In addition to these considerations, there was another important specimen design constraint. A unique facility exists at SwRI for the study of cracking phenomena. This facility is a low frequency cyclic loading stage which operates in the Scanning Electron Microscope (SEM) [1]. The maximum load capacity for this device is about 4000N (900 pounds) and since the superalloy selected for study has very high strength, the cross sectional area of the specimen was necessarily limited. The dimensional limitations of the cyclic stage also limited the overall length and width somewhat, but this was not an important consideration. Working within all these constraints, the specimen shown in Figure 1 was designed. A 25.4 x 50.8 x 76.2 mm block of IN-100 was shipped to Varian, Inc., who, using a multi-wire wafering machine, sliced the material into specimen blanks 19.0 x 50.8 x 1.27 mm. (At the same time, a second superalloy, conventionally processed Rene´ 95 was also cut into the same size blanks. It was intended to use this second material for comparison purposes if circumstances would allow it.) The wafering process was used partly because it produced a large number of blanks relatively cheaply, but more importantly, the wafering process introduces little or no surface damage. The blanks were then prepared according to Figure 1 except that the initial center hole was only 3.18 mm in diameter. This small center hole was used in the three-point bending fatigue rig used to initiate the crack. Once the crack was identified, the center of the specimen was removed by

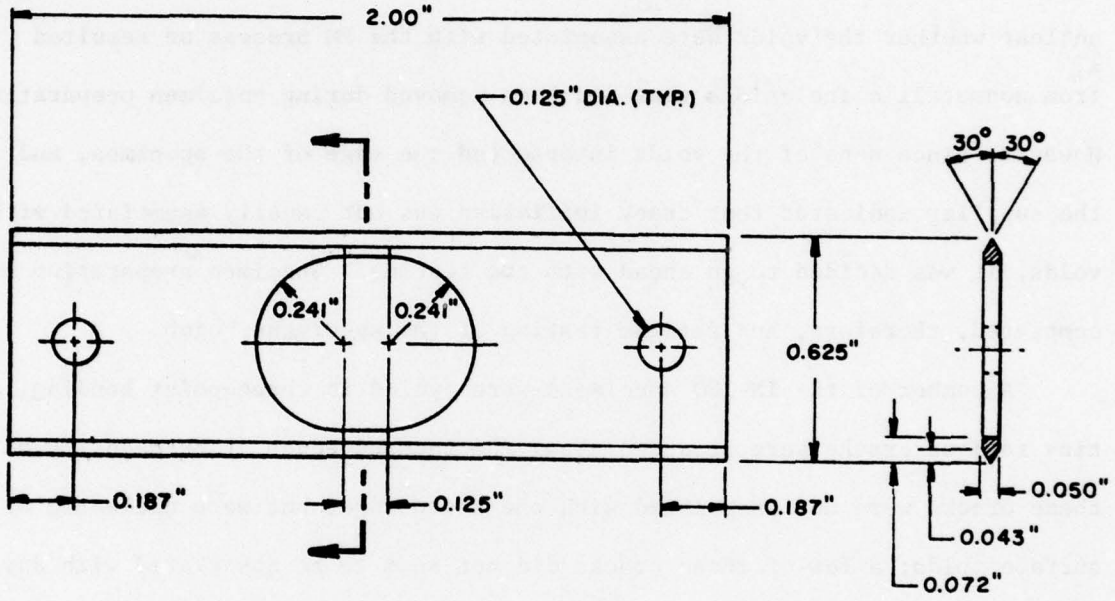

Figure 1. Schematic of Fatigue Specimen

Electro-Discharge Machining (EDM) to achieve the final configuration of Figure 1.

During the preparation of the tapered edges on the specimens, a number of voids were noted on the surface of the material. At this time, it was unclear whether the voids were associated with the PM process or resulted from nonmetallic inclusions that had been removed during specimen preparation. However, since none of the voids intersected the edge of the specimen, and the supplier indicated that crack initiation was not usually associated with voids, it was decided to go ahead with the testing. Specimen preparation was completed, therefore, and fatigue testing of the specimens begun.

A number of the IN-100 specimens were cycled in three-point bending, and tiny fatigue cracks were produced along the tapered edges. The majority of these cracks were not associated with the sharp edge, but were nucleated at surface voids; a few of these cracks did not seem to be associated with any defect. Figure 2 shows an example of two cracks emanating from a void located below the edge of the specimen. When first located, the cracks were 4-15 microns long; once identified, no further growth was observed in any of the cracks even after several hundred thousand cycles.

There are several possible reasons for the failure of the cracks to grow. It is possible that when the cracks made the transition from the Stage I (shear along crystallographic planes) initiation mechanism to a deformation mode resembling macroscopic Mode I opening (opening parallel to the applied load), the stress intensity factor of this new Mode I crack was simply below the crack propagation threshold. Because of the geometry, it is difficult to estimate the stress intensity, but if we assume the geometry of a 0.15 μm through crack as a worst case, and the applied stress on the crack is equal to the yield stress, then $\Delta K = 7.7$ MPa$\sqrt{m}$ (7.0 ksi$\sqrt{in.}$), which is slightly

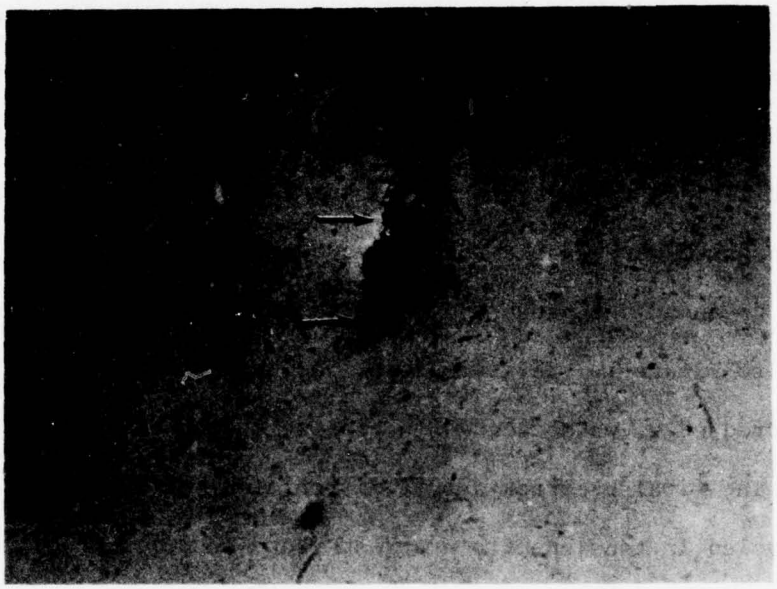

Figure 2. Surface Void Near Edge Containing Crack
(Arrows Indicate Crack Initiating from Void)

less than the room temperature threshold of IN-100. Small changes in the geometry or stress level would lower the intensity factor even further below the threshold. Similarly, the initiation event may have been associated with the stress concentration around the void; as the crack grew out of this local field, the stress intensity dropped below threshold and the crack arrested. In addition, we observed a considerable amount of microslip on the surface of the specimen; this could have caused sufficient hardening to make it impossible for the small crack to generate enough crack tip opening to propagate.

Although we were unable to propagate the cracks in bending, it was decided to go ahead and prepare a tensile specimen by enlarging the center hole to conform to Figure 1. This was done, and by carefully polishing away material at the tapered edge, we succeeded in placing the crack at the edge of the specimen. The final precrack was 12 microns long on the surface. The specimen was then cycled in tension with a stress range of 807.3 MPa (117 ksi) at R = 0.05 for 20,000 cycles. No growth was observed and the stress range was raised to 855.6 MPa (124 ksi). Following an additional 15,000 cycles, the specimen broke completely in half. The original fatigue crack did not extend during the test; the failure initiated at the edge of the center hole in the plane of the minimum section. At first it was thought that the failure originated at a surface scratch or a machine mark, but examination of the failure surface in the SEM showed the origin to be a subsurface void, approximately 0.025 mm in diameter. Surrounding the void was an area of crystallographic fracture; this was followed by an area of striations, and finally the dimpled region where ductile rupture began.

Because of the difficulty experienced in obtaining a specimen with a natural microcrack, it was decided to see if a small flaw could be created by shortening a macrocrack. A double edge notch fatigue specimen was prepared

from one of the IN-100 blanks. It was intended to load shed the specimen and obtain a small plastic zone so that, by careful machining, a small crack with a small plastic zone could be produced. However, the crack initially propagated very rapidly so that there was insufficient material remaining in the ligament to complete the load shedding. The specimen was fractured, and an examination of the fracture surface showed that the fatigue crack had initiated at a subsurface void just ahead of the machined notch. The linkup and growth of the cracks associated with this void had resulted in the rapid growth observed. Numerous other voids were visible on the fracture surface; one of these was almost 0.13 mm in diameter. All the voids examined showed similar planar facets inside the void. This indicated that surfaces of powder particles were being observed; these surfaces had not been bonded together during the processing, and thus we concluded that the observed voids resulted from the PM process and were not associated with inclusions.

2. Impact of Material Voids on Specimen Design

These tests raised serious questions about the reported lack of a role of the voids in crack initiation in a PM superalloy. In order to obtain additional evidence, several low cycle fatigue specimens were obtained from the Government Products Division of Pratt and Whitney Aircraft and their failure surfaces examined. While some of the surfaces were too abraded to examine, at least one specimen had initiated its fatigue crack at a subsurface void of approximately 0.025 mm diameter.

The discovery that in some instances subsurface voids of this size were playing a role in fatigue crack initiation led to a reexamination of the program methods. Since the size of the cracks nucleated at the voids, when combined with the void initiation sites, was on the order of 25-50 microns, this meant that attempts to propagate natural cracks 15 microns in length

would not be possible when the former cracks existed. Two alternate approaches were suggested. It might be possible to obtain microcracks that would propagate if a different material were used. The second approach would be to abandon natural initiation and obtain the small cracks through the shortening of a macrocrack. Since we already had a supply of specimen blanks of Rene´ 95, a conventionally processed superalloy, it was decided to examine its fatigue behavior. Rene´ 95 has much larger grains, 125 microns; its microstructure contains large carbide particles, which, it was feared, would influence the crack initiation process in a way similar to that of the voids in the IN-100. To check this, several three-point bending specimens were prepared and tested. The fracture of these specimens is discussed in a later section. However, at or near the fatigue crack origin of all three bending specimens, there were carbide inclusions. This led us to conclude that the carbides are inherently linked to the crack initiation process in the Rene´ 95. Even if the crack itself originates in the matrix, there will be an inclusion nearby to influence the process.

The results of this test showed that, at least as far as natural initiation was concerned, the carbides would be as troublesome in the Rene´ 95 as the voids were in the IN-100. It was suggested that another powder metallurgy superalloy be tried, but it appeared that all advanced PM alloys suffer the same problem. During processing, the hot isostatic pressing (HIP) removes any voids in the material, but heat treatment of the billet reintroduces the voids. Gatorizing does not include HIP, so some voids remain. This means that voids will be, at least some of the time, linked to the crack initiation process in the PM materials.

3. Alternate Specimen Design

The results of the preliminary study indicated that, desirable as natural microcracks might be from a technical viewpoint, it was not practical to produce them in a limited number of specimens. Therefore, it was decided to approach the problem differently, namely, to try to shorten a macrocrack to obtain a small flaw. Of course, this meant that the size of the flaw under study would have to be increased somewhat from the original goal. Since there are precision limitations in any machining process that limit the accuracy with which an operation can be performed, it is not practical to try to achieve a 15 μm crack this way. Also, because the fatigue macrocrack cannot be propagated below the threshold stress intensity factor, there is a certain inherent, minimum plastic zone size associated with whatever crack length is achieved during the machining operation. Thus, even if a very tiny crack would be machined, it would have a relatively large residual plastic zone ahead of it which probably would not be a realistic representation of a naturally occurring small crack. These considerations led us to set 0.075 mm as a goal for our shortened macrocrack and to design a new specimen.

The second specimen designed in this program is shown in Figure 3. To obtain this configuration, a 19.05 mm wide, single edge notch specimen containing a machined notch of length 5.33 mm was cycled at 5 Hz, R = 0.05, to produce a fatigue crack approximately 2.29 mm long. The initial stress intensity range was about $\Delta K = 22$ MPa$\sqrt{m}$, and as the crack grew, the load was successively reduced until the approximate room temperature threshold for IN-100, 8.8 MPa$\sqrt{m}$, was reached. During the load shedding operation, the crack growth rate was periodically monitored and found to agree with other investigators [2]. Once load shedding was complete, the specimen was then machined

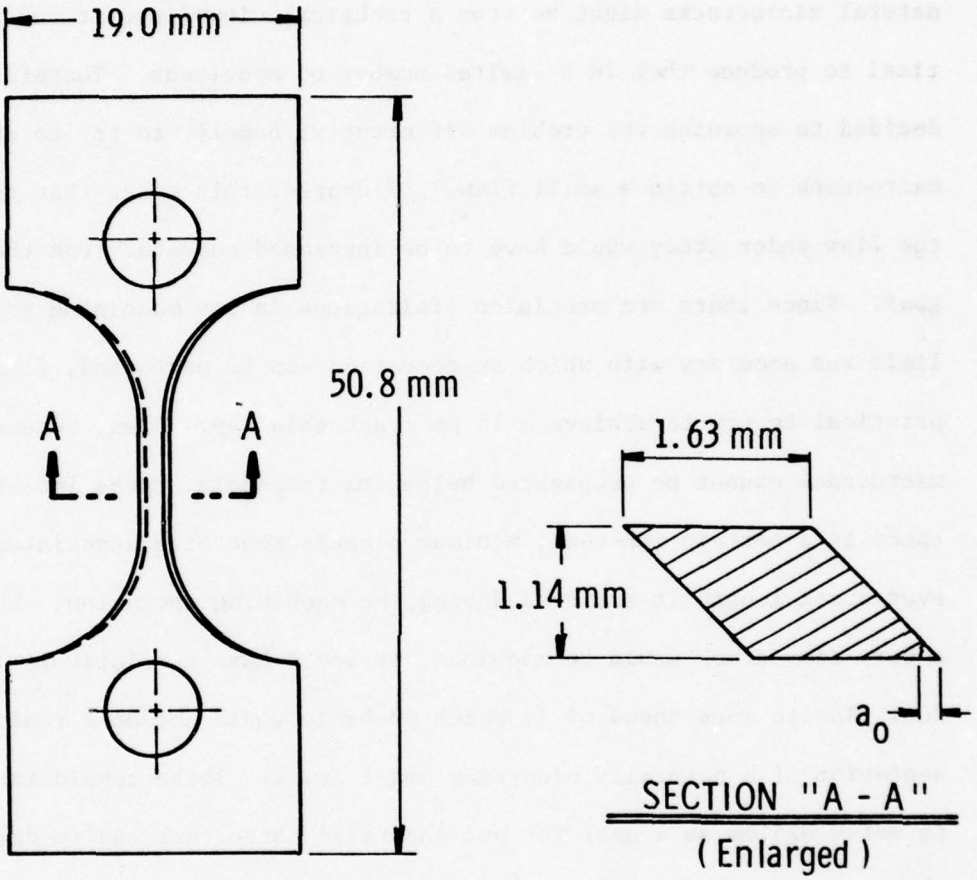

Figure 3. Final Fatigue Specimen Design

and polished into the configuration shown in Figure 3. This was accomplished by electro-discharge machining away the bulk of the material and then removing the remainder of the material using progressively finer polishes. The final polish used was 0.05 micron alumina slurry. Cracks as short as 0.06 mm were produced in this fashion.

Briefly summarizing the specimen design considerations, the original specimen, Figure 1, was abandoned because of problems associated with the crack initiation process in the PM superalloy materials. Specifically, the presence of voids in the material made the prospect of initiating and growing a single microcrack at a specific location very risky. The second specimen, was designed to utilize an existing fatigue crack. The specimen, Figure 3, resulted from load shedding a SEN specimen and subsequently machining away material to leave only the crack tip, 0.06-0.16 mm long, in the test panel. This specimen was used for all crack propagation tests.

In addition to these two specimens, a simple three-point bend specimen was used to examine the crack initiation and propagation character of Rene´ 95. These tests were qualitative in nature and are discussed later in the section on fractography.

4. Specimen Analysis

As shown in Figure 3, the cross section of the specimen was a parallelogram containing a crack at one of the acute corners. This configuration was chosen for two reasons. First, the taper allows a better definition of the crack front location. Second, a very short, through thickness crack in a rectangular cross section would interact with a great number of grains along its crack front and, because of its very short length, would not really be representative of any naturally occurring crack. The crack in the taper, on

the other hand, interacts with a much smaller amount of material along its crack front, and is somewhat more representative of a natural small crack.

The unusual geometry of this specimen makes the exact computation of the crack tip stress intensity factor difficult. While numerical analysis could have been performed, it was felt that this was not desirable in this case because of the cost and the possible lack of definition of the subsurface crack front. Instead, a simple estimation procedure was used to determine the stress intensity. Following Liu [3], symmetry arguments based on surface flaws and free surface corrections were used to arrive at a value of

$$K = 0.82\ \sigma \sqrt{\pi a} \qquad (1)$$

Moreover, because of the nonuniform gage section, there exists a stress concentration which we estimated to be seven percent.

This estimate of the stress intensity factor was subsequently verified using interferometric techniques to measure the plastic zone size associated with the crack tip. By measuring the plastic zone size in specimens of known and unknown stress intensity and comparing the results, the unknown stress intensity factor can be determined. The intensity factor obtained in this way agreed with (1) within 3 percent. The details of this procedure are given in Reference 4 and are discussed in the appendix.

5. Etching of IN-100

Since one of the goals of this program was to determine the extent of interaction between the crack tip and the microstructure, it was necessary that a technique be developed to define the microstructure. During the early stages of the program, a great deal of difficulty was experienced in doing this for the IN-100. Little information on etching this alloy is available in the open literature, and conversations with other users were of little

help. Generally, either the grain boundaries were not revealed with sufficient clarity, or else the material was so extensively attacked that, although the boundaries were visible, the material was rendered useless for testing purposes since we were unable to resolve the crack tip accurately enough to measure it. However, from this experience and from development work on standard etchants for the nickel-base superalloys, a very satisfactory etch was produced. This procedure is based on etch Number 22a in ASTM E407, Specification of Etchants and, in final form, is a 10:1 HCl to H_2O_2 (30%) solution used at room temperature. The H_2O_2 is added to the HCl and the solution is allowed to stand for approximately 15 minutes or until the solution begins to turn yellow-green. The specimen is then submerged for one minute in the etch. Figure 4 illustrates the result of this procedure. The figure shows the extremely fine grain size, 3-5 microns, and the uniformity of the material. The figure also shows that the γ' precipitates cover a large range of sizes; some are almost as large as the grain themselves, while others are barely distinguishable inside the grains. The precipitates are irregularly shaped and did not appear to congregate at any particular location, although the large precipitates are located at the grain boundaries.

Once this etch had been developed, it was possible to define the crack tip-grain boundary-precipitate interactions, at least in the SEM. An attempt was made to measure crack growth using an etched specimen, but this was abandoned. Without the resolution power of the SEM, there were too many features surrounding the crack tip for easy location; the crack tip could be located and the crack length measured, but the process was so time consuming as to be not worth the effort. The testing of etched specimens was limited to the SEM thereafter.

1300X

Figure 4. Typical Structure of IN-100. Note The Large Block γ' Precipitates At The Grain Boundaries.
Etchant: 10 HCl: 1 H_2 O_2 (30%)

SECTION III

FATIGUE CRACK GROWTH DATA

1. Experimental Technique

The specimen used in the crack growth tests has been described in the previous section and is shown in Figure 3. The manner in which the specimen was precracked and prepared was also discussed.

All but one of the fatigue tests were conducted on IN-100. Limited data on one Rene´ 95 fatigue specimen were also obtained. Nominal properties of these two materials are given in Table 1.

Because of the resolution requirements of this program, ordinary optical techniques of measuring crack advance were inadequate. Moreover, other techniques which are capable of great accuracy, e.g., electric potential, are remote measuring techniques, as well as giving average length values, and therefore would not allow the determination of crack-tip microstructure interactions as part of the measurements. Replica techniques are ordinarily used in these circumstances, but their use at elevated temperature requires that the specimen be cooled to room temperature each time a measurement is to be taken. This not only is time consuming, but also introduces a thermal fatigue cycle. Since the goal of the project was to avoid these effects whenever possible, the thermal cycles were not desirable.

In order to overcome these problems, a special high magnification, long working distance microscope was needed. Such an instrument was designed and will be described in a subsequent section.

Because of the convenience of measurement offered by the use of the microscope, it was planned to use it to monitor crack growth during the room temperature experiments, as well as those at elevated temperature. However,

TABLE 1. GATORIZED IN-100

	UTS GPa (ksi)	YS GPa (ksi)	Percent Elongation	Percent Reduction in Area
Room Temperature Tensile	1.58 (229.8)	1.10 (159.3)	24.0	25.1
704°C (1300°F) Tensile	1.22 (176.9)	1.07 (155.3)	22.0	31.6
732°C/655 MPa (1350°F/95 ksi) Rupture	38.0 hrs			
704°C/551 MPa (1300°F/80 ksi) 0.2% Creep	220.0 hrs			

Room Temperature Modulus, E = 213.8 GN/m^2 (31.0 x 10^3 ksi)

Rene´ 95

	UTS GPa (ksi)	YS GPa (ksi)	Percent Reduction in Area
Room Temperature Tensile	1.44 (209)	1.21 (175)	6.2

the delivery of the microscope was repeatedly delayed, and so an alternate technique had to be used for some of the room temperature tests. Several possibilities, including replication, were explored, but it was finally decided that sequential photographs, taken at a high enough magnification, offered the most expedient means of measuring the crack growth of the small fatigue cracks. Of course, this technique also provided a detailed record of the behavior of the fatigue crack on the surface of the specimen.

For the entire test duration, the test was halted after a specified number of cycles and the specimen removed. It was then placed in a Zeiss microscope and the crack photographed. Only one side of the specimen was photographed because the tapered surface made clear image photography of both sides difficult. The side that was not photographed was monitored visually.

The photographs were taken at a magnification of 1300X, which allowed the measurement of changes in crack length of 2.5×10^{-4} mm. During the initial testing, measurements were made every 400 cycles so that growth rates on the order of 2.5×10^{-7} mm/cycle were obtained. The photographs showed that the bulk of the surface crack propagation was Stage I. There was also considerable crack branching, with one branch arresting and the other propagating. Because of the permanent record provided by the photographs, it was possible to go back and recompute the crack length when the crack that had been under study arrested and a new branch began to propagate.

2. Elevated Temperature Experimental Technique

A major problem in this program was the ability to monitor minor increments of crack growth at elevated temperature. As noted previously, conventional techniques of crack measurement were not deemed suitable because of the unusual requirements of this program. These requirements made in situ

measurement of the crack length almost mandatory; moreover, the desire to view the crack tip meant that optical techniques had to be used.

Typical cathetometers for crack monitoring are usually restricted to magnifications of 75X and are capable of measuring to 1.0×10^{-2} mm (5.0×10^{-4} in.). To achieve magnifications greater than this, the cathetometer lens must be close to the heated specimen; this, in turn, results in image distortion and potential lens damage due to the heat. The resolution of these conflicting design requirements presented a real challenge.

In order to demonstrate the feasibility of a high resolution, long working distance (i.e., the distance from the lens to the specimen) microscope, a small study program was initiated. Utilizing available optical equipment and drawing on optics experts at the Institute, a working model of a microscope was developed. Contact was then made with a number of manufacturers concerning the detailed design of the microscope and the availability of the optical components. After a number of discussions, it was decided that it would be more economical to have the microscope constructed by an experienced optics manufacturer. The Ealing Corporation was selected for this task.

The resulting system is shown schematically in Figure 5a. The design is essentially a microscope within a microscope, in which the inner microscope focuses on the image of an objective lens and thereby produces the high magnification. The key element in the design is the objective lens itself. This lens is a 15X reflective objective manufactured by Beck Instrument Company and has a working distance of approximately 25 mm. This long working distance is achieved by use of parabolic mirrors instead of glass lenses; a sketch of the lens is shown in Figure 5b. The mirrors can be maintained at higher temperatures without fear of distortion or damage due to thermal

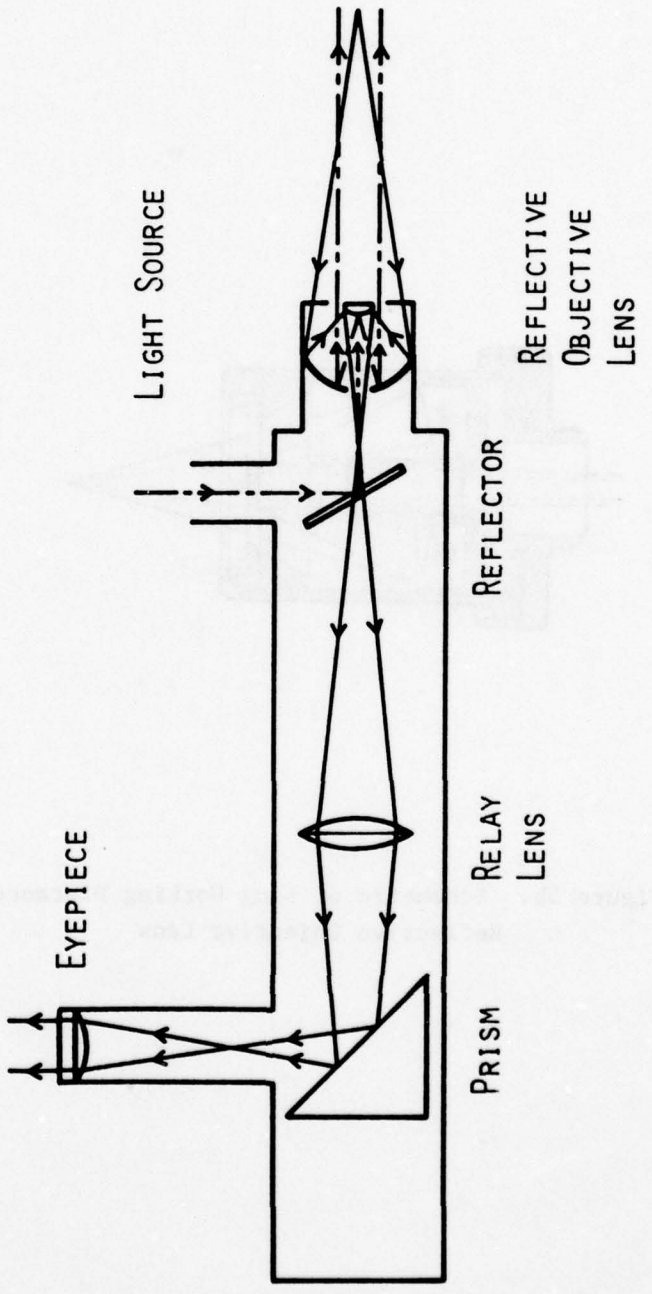

Figure 5a. Schematic of Long Working Distance Microscope

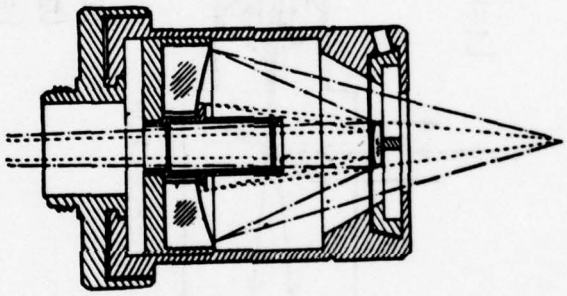

Figure 5b. Schematic of Long Working Distance
Reflective Objective Lens

expansion; this, in addition to the long working distance, significantly reduces the requirements for cooling the microscope.

The remainder of the design, the "inner" microscope, is made up of a relay lens and an eyepiece. By employing the 15X objective lens with a 5X relay lens and a 10X eyepiece, a total magnification of 600X can be achieved. The relay 5X lens can be replaced by 10X unit to achieve 1200X if it is desired.

The microscope was mounted on a triaxial translational stage with micrometer travel, as shown in Figure 6a. The entire unit was placed on a massive table weighing approximately 2150 N. Both the table and microscope were placed on isopads to minimize the vibration from the surrounding environment. Lighting was achieved by a high intensity light source in conjunction with a fiber bundle for transmission.

Because of the requirement for viewing the specimen, and because of its small thermal mass, it was decided to heat the specimen by heat conduction through the pull rods. The furnace used in this experiment consisted of two heating elements, one above and one below the specimen, which heated the pull rods but left sufficient room for viewing the crack in the specimen. Separate controllers were used for each heating element. These controllers were controlled by thermocouples attached to the top and bottom of the specimen gage section. This arrangement provided uniform heating in the gage section. However, the system does require some preliminary calibration since the thermocouples are on the specimen and the pull rods are being heated. Since the specimen is being heated by conduction, the pull rods must be heated to a slightly higher temperature than is required in the specimen. The amount of overshoot on the pull rods and the tolerance on the temperature controllers must be determined to prevent overheating the specimen.

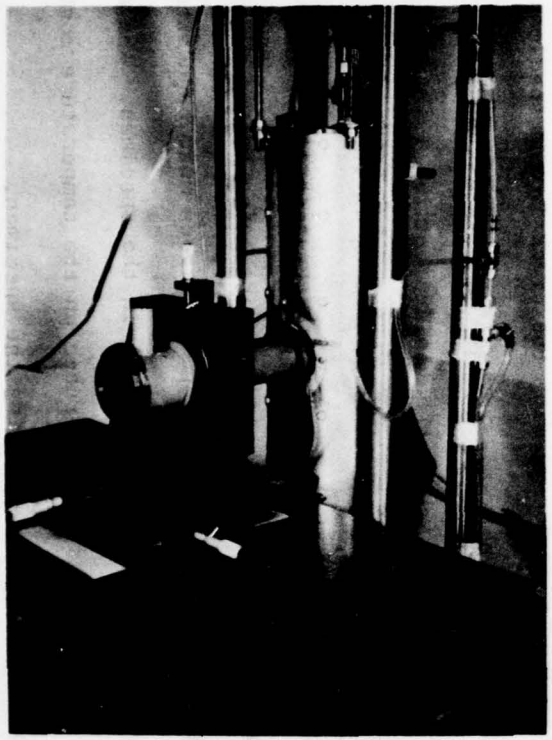

Figure 6a. Long Working Distance Microscope Interfaced With Furnace

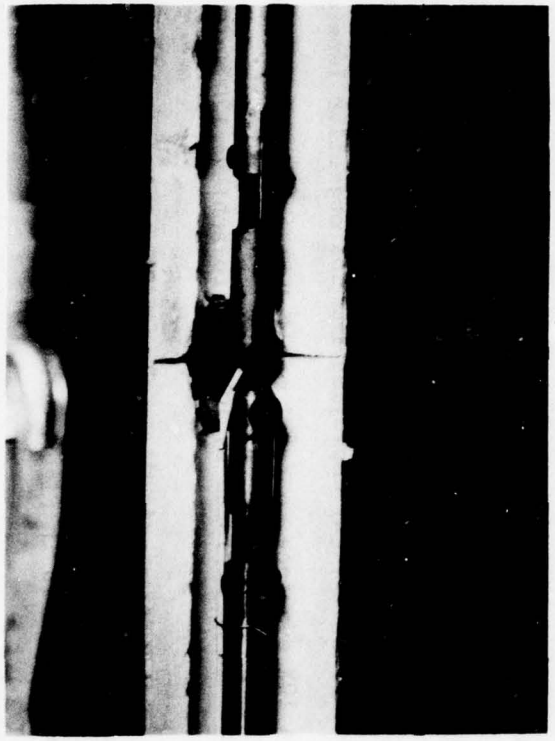

Figure 6b. Specimen and Grip Arrangement In Furnace

It should also be noted that control of the heating elements based on the temperature of the specimen resulted in somewhat larger, $\pm$ 7°C, temperature variation than is desirable. This was caused by the large difference in thermal mass between the pull rods and the specimen and the very limited heat transfer area between the two units. The pull rods heat and cool much more rapidly than the specimen and, because of the time delay of the conduction process, this results in a correspondingly larger variation in specimen temperature. In retrospect, a better system would have been to control the pull rod temperature; using the same allowable temperature variation, this would have kept the pull rods and therefore the specimen at a more nearly constant temperature. It is not expected, however, that the temperature variation during the test significantly affected the crack growth rate, particularly at this temperature. At somewhat higher temperatures where creep would be more of a factor, this would not have been true.

As shown in Figures 6a, b, the observation port was a stainless steel jacket, water cooled, with an optically ground quartz lens at the inner wall of the furnace. While not shown, air was also blown across the surface of the quartz viewport. This was done as additional insurance that the objective lens did not overheat.

After the furnace temperature had stabilized, the microscope was positioned in the observation port and the initial crack length was measured at 50 percent peak load. Cycling was begun and the length was measured after approximately 250 cycles. The cycling was stopped and the load held at 75 percent of peak load during the measurement; time for measurement was about 30 seconds. It was noted that careful handling of the specimen and all internal furnace parts was required to keep the specimen from becoming discolored. Even with care, the surface of the specimen appeared to "heat etch" after

several hours at temperature. In the case of the hold time test, the crack tip became so difficult to locate that it was necessary to twice stop the test and clean the surface.

All tests were performed in a 4.4 KN (10 kip) hydraulic fatigue machine using a 4.4 KN (1 kip) load cell; this same machine was used to precrack the specimens. The specimens were cycled under load control at a frequency of 5 Hz applied in a sinusoidal wave form. The dwell test specimen was loaded and unloaded at the same rate as the continuously cycled specimens; however, the peak stress was held for one minute.

3. Room Temperature Data

Figure 7 shows the initial portion of the graph of crack length vs cycles for specimen 2. (The test parameters for all specimens are given in Table 2.) The initial crack length in this specimen was 0.076 mm (0.003 in.). This crack started to grow immediately, increasing almost 2.5×10^{-3} mm (1.0×10^{-4} in.) in the first 400 cycles. The crack grew in a very discontinuous manner, with periods of no growth followed by sudden jumps in the crack length. There are also periods when the crack appears to be growing continuously. A striking feature of this plot is that, on this scale, a straight line fits the data very well. During the interval shown, the crack grew 0.051 mm (0.002 in.) on the surface in 22,000 cycles, for an average growth rate of 2.3×10^{-6} mm/cycle (9.1×10^{-8} in/cycle). The figure shows that there were intervals when the growth rate exceeded this by a considerable amount.

When the entire test data are plotted on the same scale, the linear crack growth behavior exists at much longer crack lengths, although the slope becomes progressively steeper. That is, following a period of constant da/dN such as shown in Figure 7, there is a gradual transition to another constant slope region, but with a steeper slope. The discontinuous growth pattern also remained, even for cracks which would be termed macrocracks.

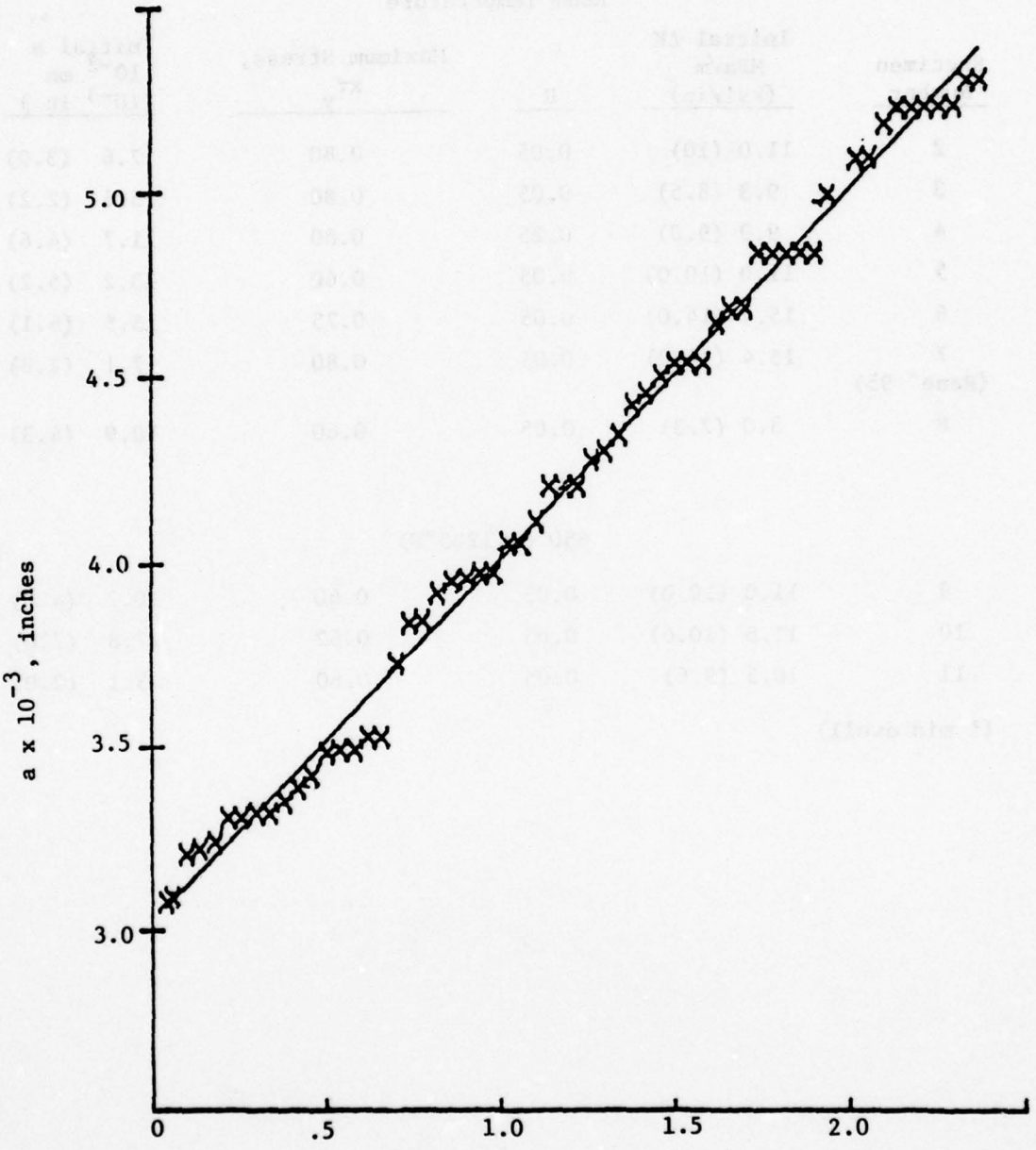

Figure 7. A Vs N Data of Specimen No. 2, R = 0.05.
(See Table 2 For Test Parameters)

TABLE 2. TEST PARAMETERS

Specimen Number	Initial ΔK MPa$\sqrt{m}$ (ksi$\sqrt{in}$)	R	Maximum Stress, $x\tau_y$	Initial a 10^{-2} mm (10^{-3} in.)
Room Temperature				
2	11.0 (10)	0.05	0.80	7.6 (3.0)
3	9.3 (8.5)	0.05	0.80	5.6 (2.2)
4	9.9 (9.0)	0.25	0.80	11.7 (4.6)
5	11.0 (10.0)	0.05	0.60	13.2 (5.2)
6	15.4 (14.0)	0.05	0.75	15.5 (6.1)
7 (Rene´ 95)	15.4 (14.0)	0.05	0.80	7.1 (2.8)
8	8.0 (7.3)	0.05	0.60	10.9 (4.3)
650°C (1200°F)				
9	11.0 (10.0)	0.05	0.60	10.2 (4.0)
10	11.6 (10.6)	0.05	0.62	17.8 (7.0)
11	10.5 (9.6)	0.05	0.80	5.1 (2.0)

(1 min dwell)

In attempting to reduce the data to crack growth rate values, or even to assess the significance of the constant growth rate regimes, the question of the scale of the observation must be considered. That is, if the data shown in Figure 7 are used, then a smooth polynomial curve fit to each of the points would result in large variations in the growth rates. This would yield statistical information about the maximum and minimum growth rates achieved over a period of time. Essentially, however, this analysis is trying to fit the discontinuous process of crack advance with a continuous analysis. The range of the parameters shown in Figure 7 is very expanded, but on the other hand, if the scale selected is too small, the data will be so compressed that all the features are wiped out and a simple parabola can fit the data.

Figure 8 shows the results of two crack data analyses using different scales. The first, 8a, shows the crack growth data resulting from selecting points at crack length intervals of 0.013 mm (0.0005 in.) and then calculating average growth rates over the interval. This process results in some scatter, as the essential discontinuous nature of the process is retained. The data show a factor of 2-3 covering the scatter in growth rate. Note also that the behavior persists at high ΔK where it might be anticipated that the large crack and plastic zone would combine to render the growth process almost continuous.

The second plot, 8b, shows the same set of data, except that only half as many points were selected; that is, the crack length interval used this time was 0.025 mm (0.001 in.). While the same trend is maintained, the effect has been to smooth the data drastically. Note that the data do not now convey the discontinuous cracking process. However, they do show an average growth rate which would be more useful in computing the lifetime of a structure. Since the bulk of crack growth measurements are made at this or

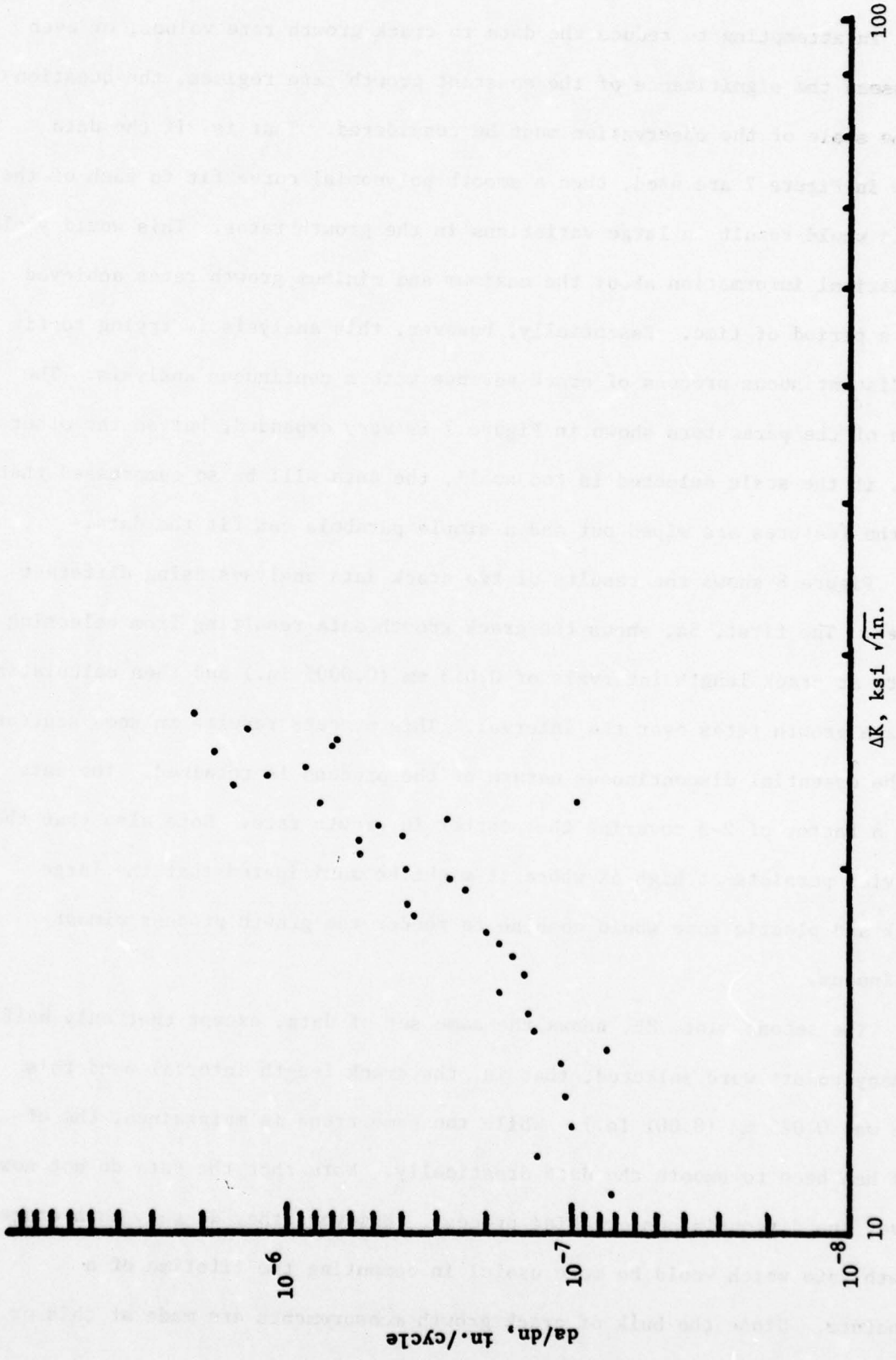

Figure 8a. Crack Growth Rate Vs Stress Intensity Factor
For Specimen 2, R = 0.05.
(See Table 2 For Test Parameters)

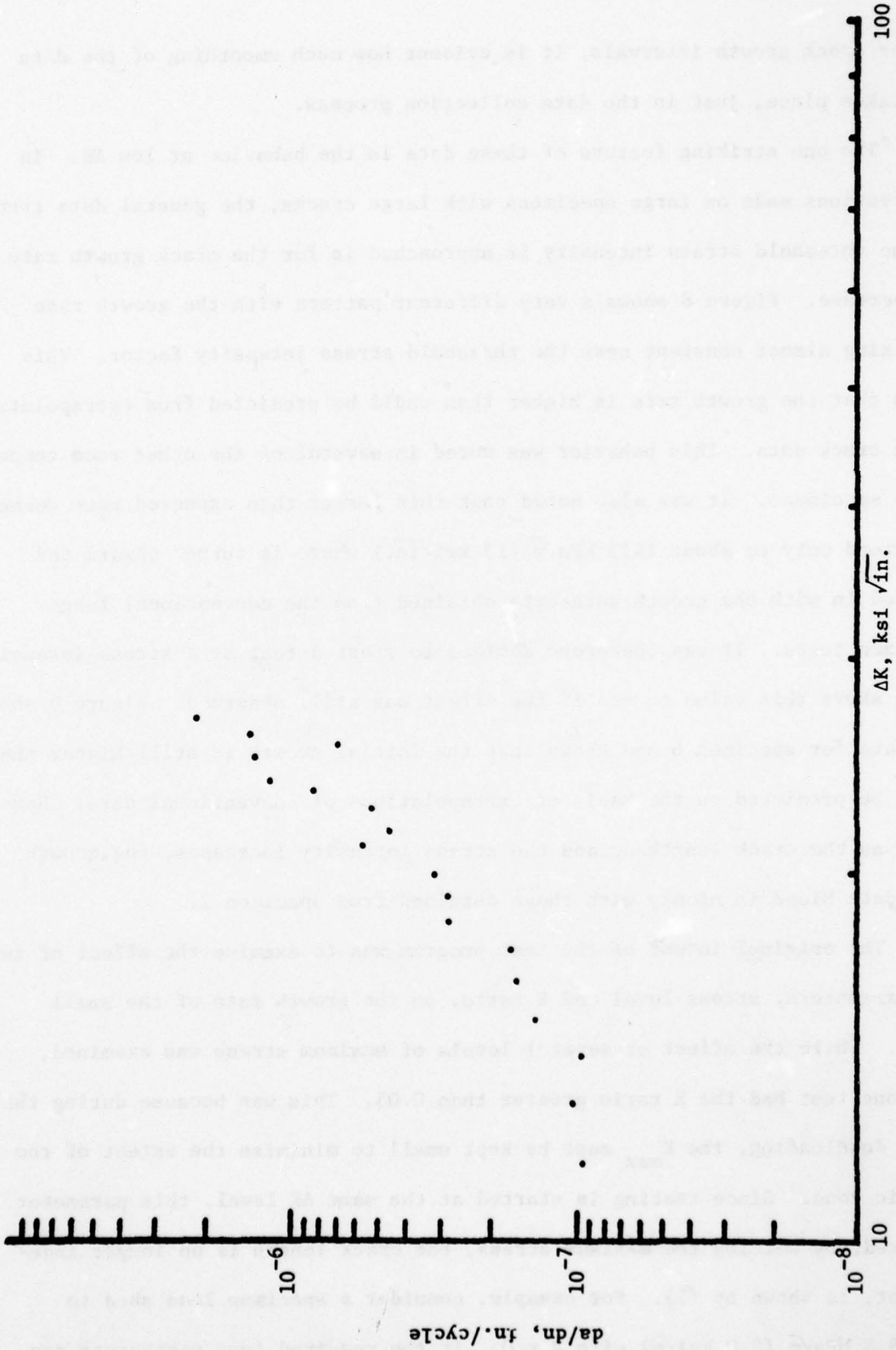

Figure 8b. Crack Growth Rate Vs Stress Intensity Factor
For Specimen 2, R = 0.05
(See Table 2 For Test Parameters)

larger crack growth intervals, it is evident how much smoothing of the data has taken place, just in the data collection process.

The one striking feature of these data is the behavior at low ΔK. In observations made on large specimens with large cracks, the general data trend as the threshold stress intensity is approached is for the crack growth rate to decrease. Figure 8 shows a very different pattern with the growth rate remaining almost constant near the threshold stress intensity factor. This means that the growth rate is higher than would be predicted from extrapolating large crack data. This behavior was noted in several of the other room temperature specimens. It was also noted that this faster than expected rate seemed to extend only to about 14.3 MPa$\sqrt{m}$ (13 ksi$\sqrt{in.}$) where it turned upward and blended in with the growth rate data obtained from the conventional large specimen tests. It was therefore decided to start a test at a stress intensity range above this value to see if the effect was still observed. Figure 9 shows the data for specimen 6 and shows that the initial growth is still higher than would be predicted on the basis of extrapolations of conventional data. However, as the crack lengthens and the stress intensity increases, the growth rate data blend in nicely with those obtained from specimen 2.

The original intent of the test program was to examine the effect of two key parameters, stress level and R ratio, on the growth rate of the small flaws. While the effect of several levels of maximum stress was examined, only one test had the R ratio greater than 0.05. This was because during the final downloading, the K_{max} must be kept small to minimize the extent of the plastic zone. Since testing is started at the same ΔK level, this parameter is fixed; by setting the maximum stress, the crack length is no longer independent, as shown by (1). For example, consider a specimen load shed to ΔK = 8.8 MPa$\sqrt{m}$ (8.0 ksi$\sqrt{m}$) with R = 0. If the required test parameters are

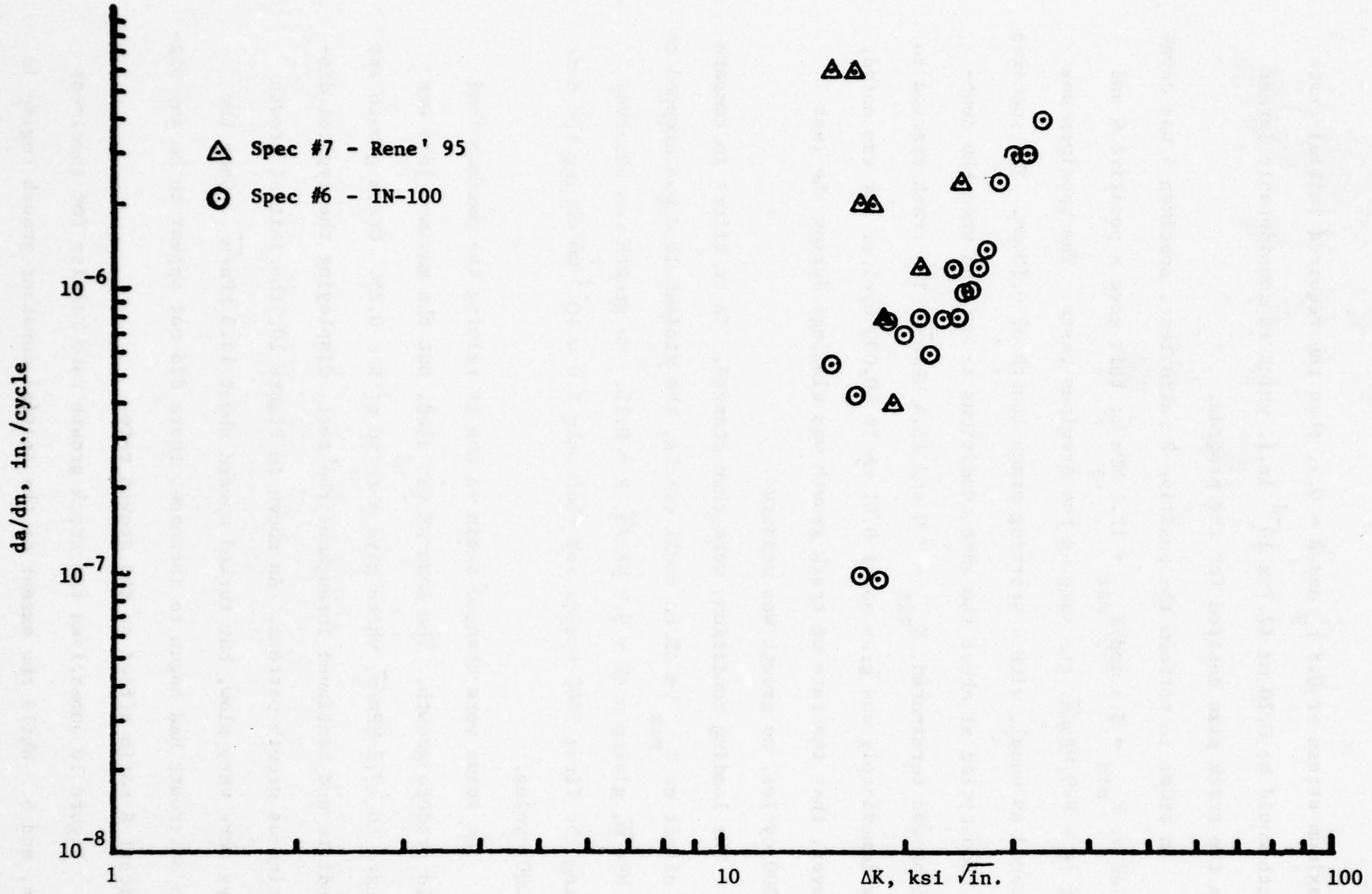

Figure 9. Crack Growth Rate Vs Stress Intensity Factor For Specimens 6 and 7. (See Table 2 For Test Parameters)

a maximum stress of 0.8 τ_y and R = 0.5, then the required initial crack length would be 0.20 mm (7.7×10^{-3} in.), which is considerably larger than the crack size desired for the program.

In order to perform the positive R ratio test, specimen 4 was downloaded to K_{min} = 3.3 and K_{max} = 12.1 MPa$\sqrt{m}$; this gave a positive R and kept ΔK = 8.8 MPa$\sqrt{m}$, the same as the previous tests. The specimen was prepared as usual, with a starting crack length of 0.10 mm. The specimen was then cycled at about the same conditions as existed when the downloading was terminated, K_{min} = 3.0 and 11.4 MPa$\sqrt{m}$. The crack started to grow immediately and grew about 0.01 mm in 60,000 cycles. It was noted, however, that the rate of crack growth was slowing; during the last 25,000 cycles, no growth was measured.

The loading conditions were then changed. In an effort to compare the effect of K_{max} vs ΔK on small cracks, the minimum load was dropped to 1.5 MPa$\sqrt{m}$, giving a ΔK = 9.9 MPa$\sqrt{m}$, R = 0.13. No growth was observed during the first 5000 cycles and then only 1.0×10^{-3} mm during the next 25,000 cycles.

The loads were changed again to see if raising the maximum load would produce growth. The same ΔK was used, but the maximum load was changed to 13.2 MPa$\sqrt{m}$, which gave a ratio of R = 0.25. Crack growth was immediate and continued throughout the test, displaying the typical discontinuous growth pattern. As shown in Figure 10, the initial growth rates were very slow, but turned upward about 14.3 MPa$\sqrt{m}$. Once the rate of growth had begun to increase, there did not appear to be any significant R ratio effect on the growth rate.

Figure 10 summarizes the crack growth rate results for specimens 3, 4, and 5. While the extent of the initial constant growth regime is

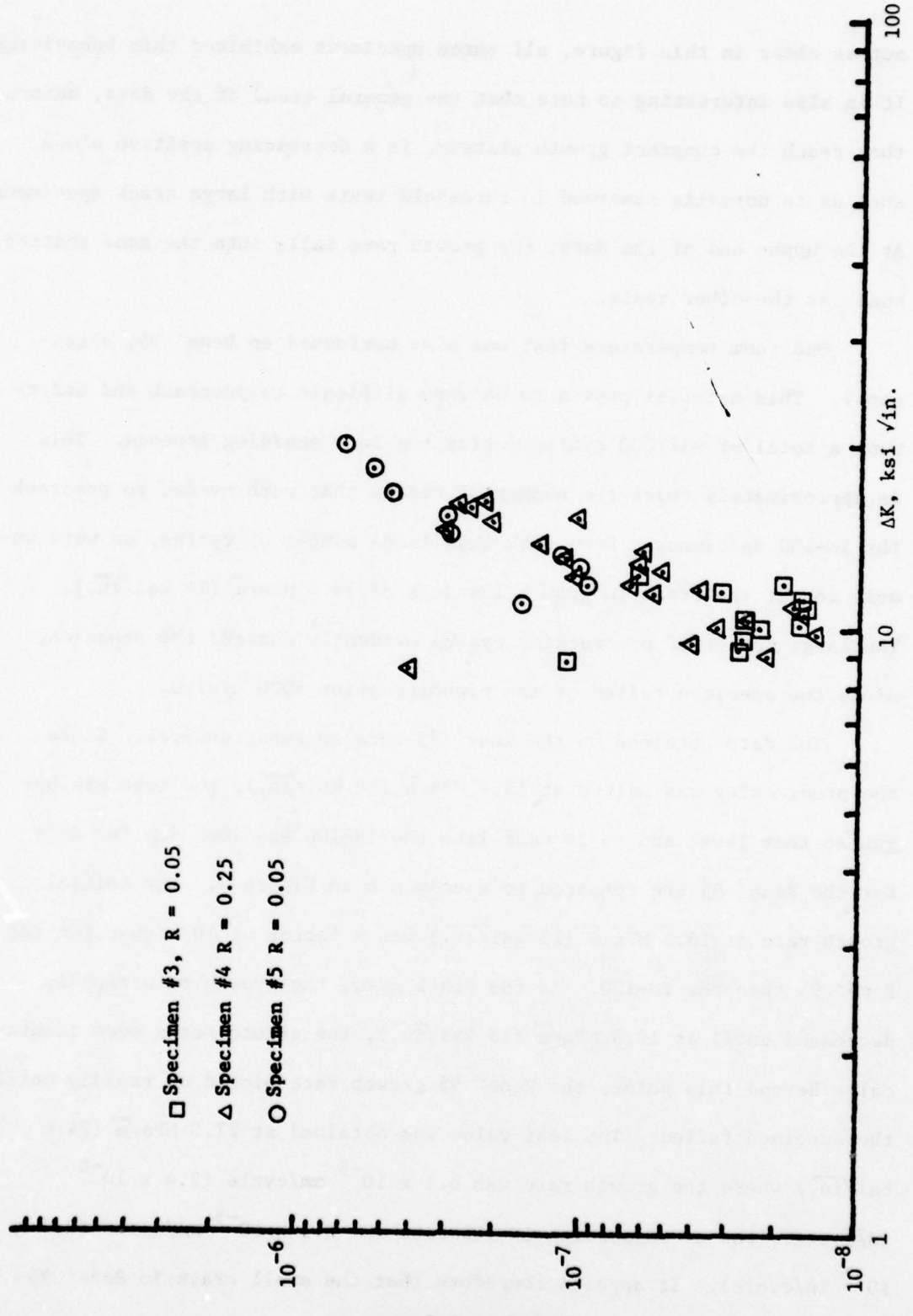

Figure 10. Crack Growth Rate Vs Stress Intensity Factor For Specimens 3, 4, and 5. (See Table 2 For Test Parameters)

not as clear in this figure, all three specimens exhibited this behavior. It is also interesting to note that the general trend of the data, before they reach the constant growth plateau, is a decreasing positive slope such as is normally observed in threshold tests with large crack specimens. At the upper end of the data, the growth rate falls into the same scatter band as the other tests.

One room temperature test was also performed on Rene´ 95, specimen 7. This material proved to be very difficult to precrack and underwent a total of 937,000 cycles during the load shedding process. This is approximately twice the number of cycles that were needed to precrack the IN-100 specimens. Even with this large number of cycles, we were unable to get the crack to grow below a ΔK of 15.4 MPa$\sqrt{m}$ (14 ksi$\sqrt{in.}$). The large number of precracking cycles evidently damaged the pinholes, since the specimen failed at the pinholes after 5000 cycles.

The data obtained on the Rene´ 95 were somewhat unusual. Since the precracking was halted at 15.4 MPa$\sqrt{m}$ (14 ksi$\sqrt{in.}$), the test was begun at that level and so is most like the IN-100 specimen 6. The data for the Rene´ 95 are compared to specimen 6 in Figure 9. The initial growth rate at 16.5 MPa$\sqrt{m}$ (15 ksi$\sqrt{in.}$) was a factor of 10 higher for the Rene´ 95 than the IN-100. As the crack grew, the growth rate rapidly decreased until at 19.8 MPa$\sqrt{m}$ (18 ksi$\sqrt{in.}$), the growth rates were identical. Beyond this point, the Rene´ 95 growth rate picked up rapidly until the specimen failed. The last value was obtained at 27.0 MPa$\sqrt{m}$ (24.6 ksi$\sqrt{in.}$) where the growth rate was 6.1×10^{-5} mm/cycle (2.4×10^{-6} in/cycle); the corresponding IN-100 rate was 2.3×10^{-5} mm/cycle (9.0×10^{-7} in/cycle). It appears therefore that the small crack in Rene´ 95 was growing more quickly than in the IN-100 over the bulk of the load

regime. However, because of the unusual nature of the Rene´ 95 data, this should be treated as more speculation than conclusion.

Figure 11 summarizes the room temperature fatigue crack growth data and compares these data with some Pratt and Whitney data [5]. The agreement among the small crack tests is excellent. It is especially encouraging that the slopes are in fairly good agreement since they are computed over a fairly narrow range of data. The results also show good agreement with the conventional large specimen IN-100 results.

4. Elevated Temperature Data

Three elevated temperature tests were run on the IN-100 material. Two were run under sinusoidal loading, while the third was cycled at the same rate, but included a one minute dwell at maximum load. All tests were run at 650°C (1200°F). The maximum stress initially was 620-655 MPa (90-95 ksi), so creep should not have affected the growth rate until the crack had grown considerably. Because of the small size of the specimen and the high growth rate at the elevated temperature, it was possible to make a limited number of measurements, so the data base is somewhat limited.

The three specimens were all precracked at room temperature. Specimens 9 and 10 were run to duplicate the room temperature tests, both starting with a ΔK of about 10. As shown by Figures 12 and 13, specimen 9 had a somewhat lower growth rate, but it is within the normal factor of two scatter associated with fatigue crack propagation. Specimen 9 also has a somewhat lower slope, but the data obtained from this test were over a very limited range.

The results of the hold time test, No. 11, are also shown in the two figures. There is no difference in growth rate between it and the

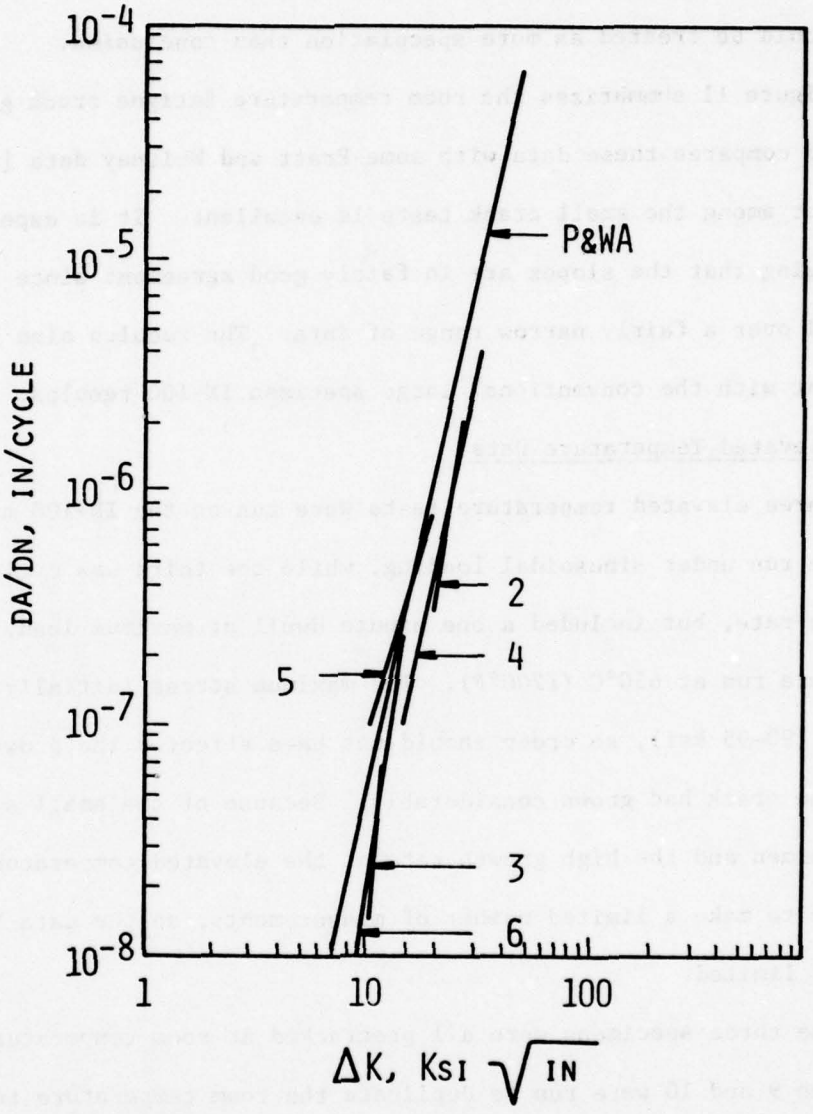

Figure 11. Summary of Room Temperature Fatigue Crack Growth Rate Data (See Table 2 For Test Parameters)

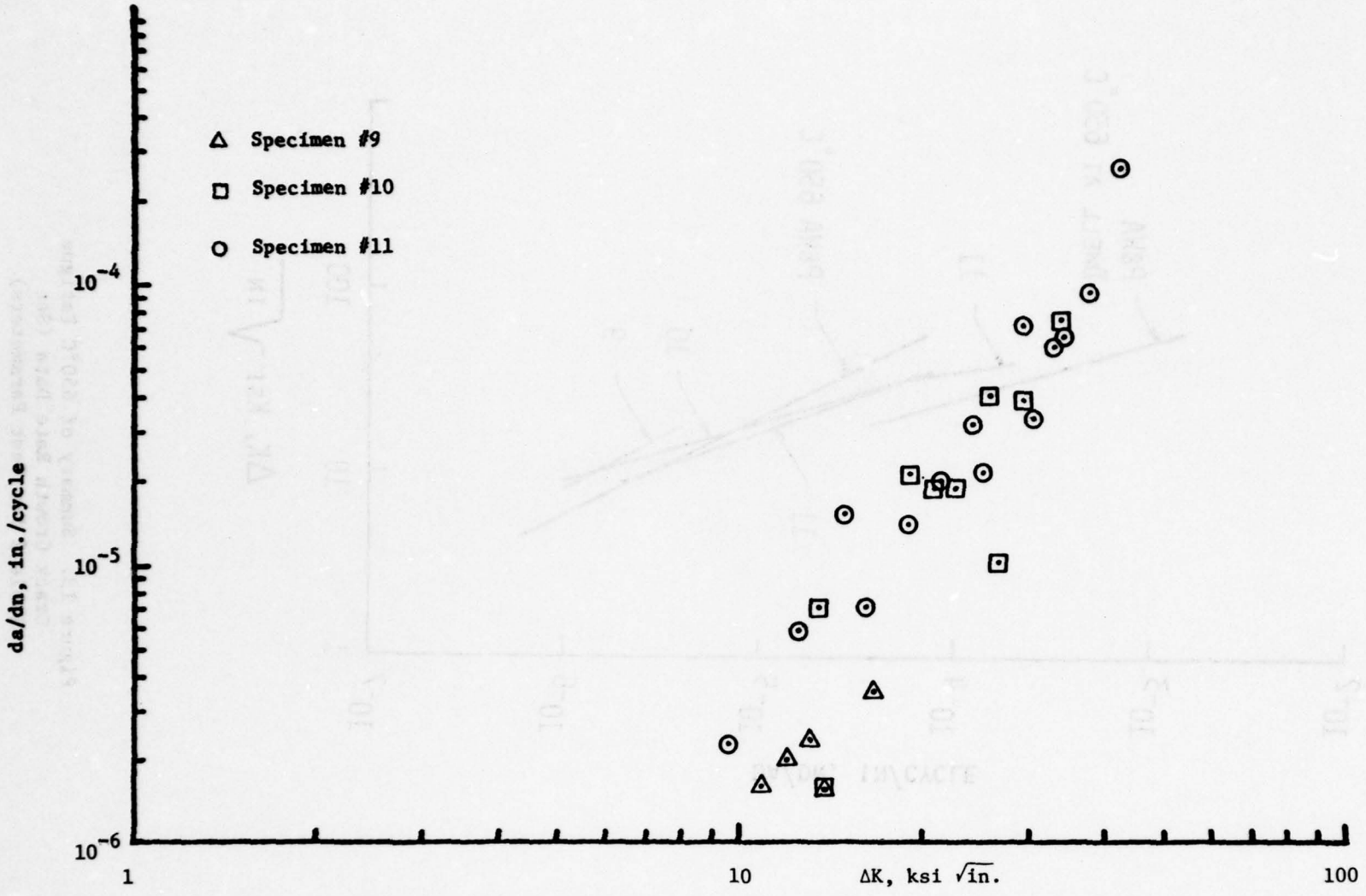

Figure 12. Crack Growth Rate Vs Stress Intensity Factor For Specimens 9, 10, and 11. (See Table 2 For Test Parameters)

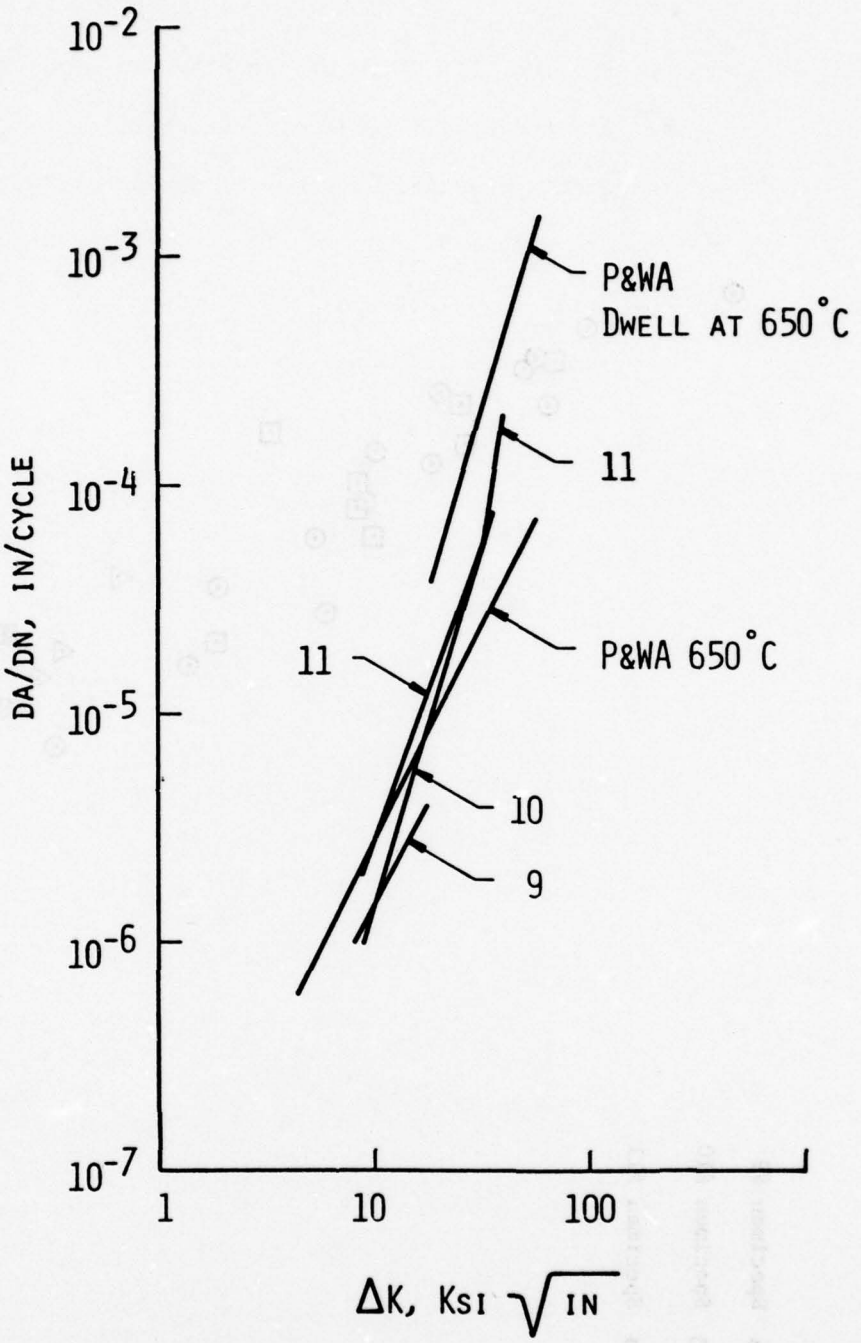

Figure 13. Summary of 650°C Fatigue Crack Growth Rate Data (See Table 2 For Test Parameters)

sinusoidal specimen, No. 10. All three of the elevated temperature tests fall within the same scatter band. It is also interesting to observe that there is no trace of a constant growth rate period exhibited by the elevated temperature specimens.

Figure 13 shows that two sinusoidal crack growth rates agree quite well with the reported data [2] for large specimens, although the slope of specimen 10 is somewhat larger than the Pratt and Whitney data. The major disagreement is in the hold time test, where the current data are about a factor of 5 slower than the large specimen hold time test. Even late in the test, when the growth rate for specimen 11 is accelerating due to the decrease in cross section, the values of da/dN are still below the data of [2]. The measurements made in [2] incorporated a thermal cycle as the specimens were cooled before the crack lengths were measured. Thus it is unclear whether the disagreement represents a small crack effect or the effect of experimental technique. This point will be discussed in a subsequent section.

SECTION IV

SEM OBSERVATIONS

In the following sections are reported the results of fractographic analyses of broken specimens, as well as optical microscopy of surface crack paths and in situ SEM surface observations of crack tips under dynamic cycling conditions.

1. Fractography

Fractographic observations were carried out on specimens fractured under a variety of conditions, including: (1) low cycle fatigue (LCF) of cylindrical specimens of IN-100 (tests carried out, and specimens provided, by Pratt and Whitney Aircraft); (2) room temperature fatigue fracture of a center hole razor blade IN-100 specimen; (3) room temperature fatigue fracture of standard double-edge-notched (DEN) IN-100 specimen; (4) room temperature fatigue fracture of Rene´ 95 bending specimens; (5) room temperature fatigue failure of precracked , reduced section IN-100 razor blade specimens; (6) high temperature fatigue failure of precracked , reduced section IN-100 razor blade specimens. In this section, the fractography of each situation is described in detail.

a. LCF Tests of IN-100

Three LCF fractures of IN-100 specimens were examined in detail. One of the pairs of fracture surfaces had brinelled to the extent that no details could be seen, so attention was focused on the two remaining specimens. In one specimen, tested at 538°C, the origin of fracture was a subsurface region of incomplete sintering (Figure 14). In another specimen, tested at room temperature, the origin was composed of a pair of slightly subsurface voids, which caused the thumbnail-shaped

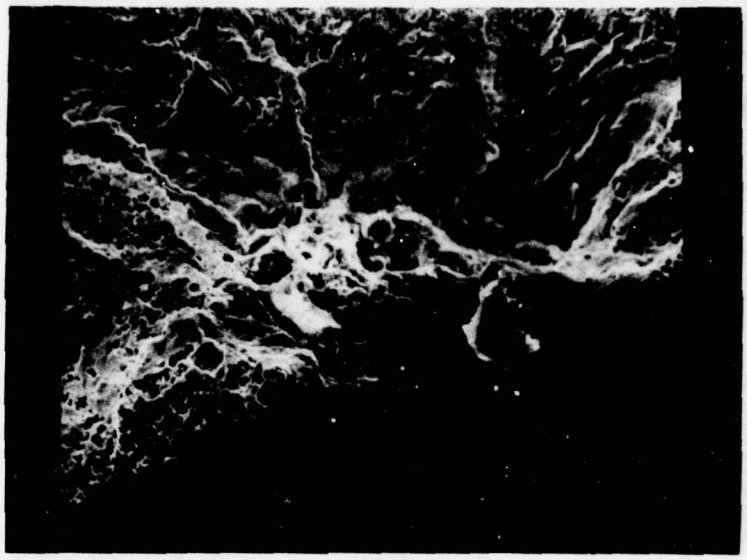

Figure 14. Initiation Site in LCF Specimen Resulting From Unsintered Material. 600X

Figure 15a. Thumb Nail Fatigue Crack in LCF Specimen. 26X

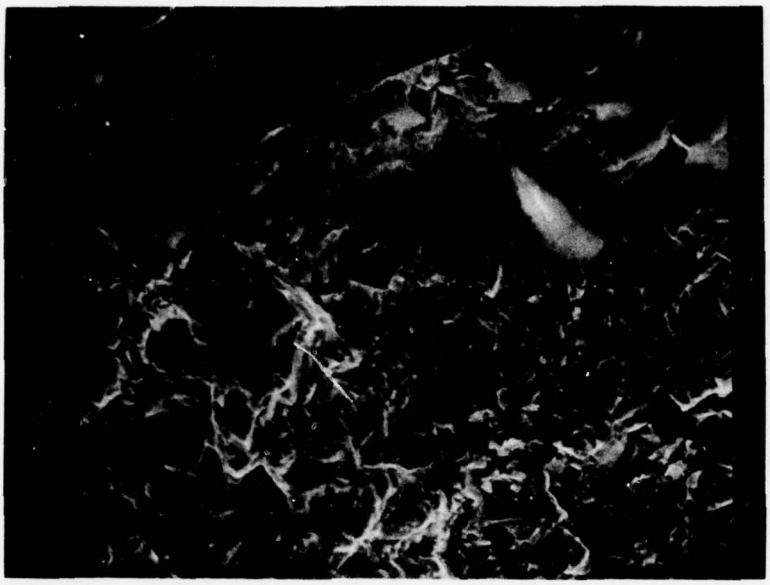

Figure 15b. Voids Located At Initiation Site. 1004X

Figure 15c. Close View of Voids. 2600X

crack shown in Figure 15a. Higher magnification views of the two voids are shown in Figure 15(b and c), in which fatigue striations also can be seen adjacent to the holes.

b. Room Temperature Fatigue Fracture of Center Hole Razor Blade IN-100 Specimen

Cracks were introduced into this specimen by bending, as described elsewhere; this specimen is shown in Figure 1. One such specimen with a 12 μm crack in the taper was obtained, transferred to a tension fatigue rig and cycling resumed. The specimen failed in 36,000 cycles, with the origin of failure being at the edge of the center hole, rather than, as anticipated, along the taper at one of the original microcrack sites. As in the Pratt and Whitney specimens, the origin of the failure was found to be a subsurface void (Figure 16). The void was located in the minimum section, such that the K_T of the center hole, together with that of the void itself, led to a crack which dominated the precrack at the edge of the specimen. It should be noted that in this case the void was located in an area of crystallographic fracture, rather than a striated region, as for the LCF tests. The voids, incidentally, are quite hard to spot when the surrounding region is crystallographic, since the voids themselves are faceted.

As sketched in Figure 17, the region of crystallographic "cleavage" containing the initiating void first is followed by an area of mixed cleavage and striations, then by a region consisting principally of striations, and finally by the dimples characteristic of rapid crack growth. It will be shown that these transitional trends in fractography are repeated for the small crack tests.

Figure 16. Void At Initiation Site of Razor Blade Specimen. 1700X

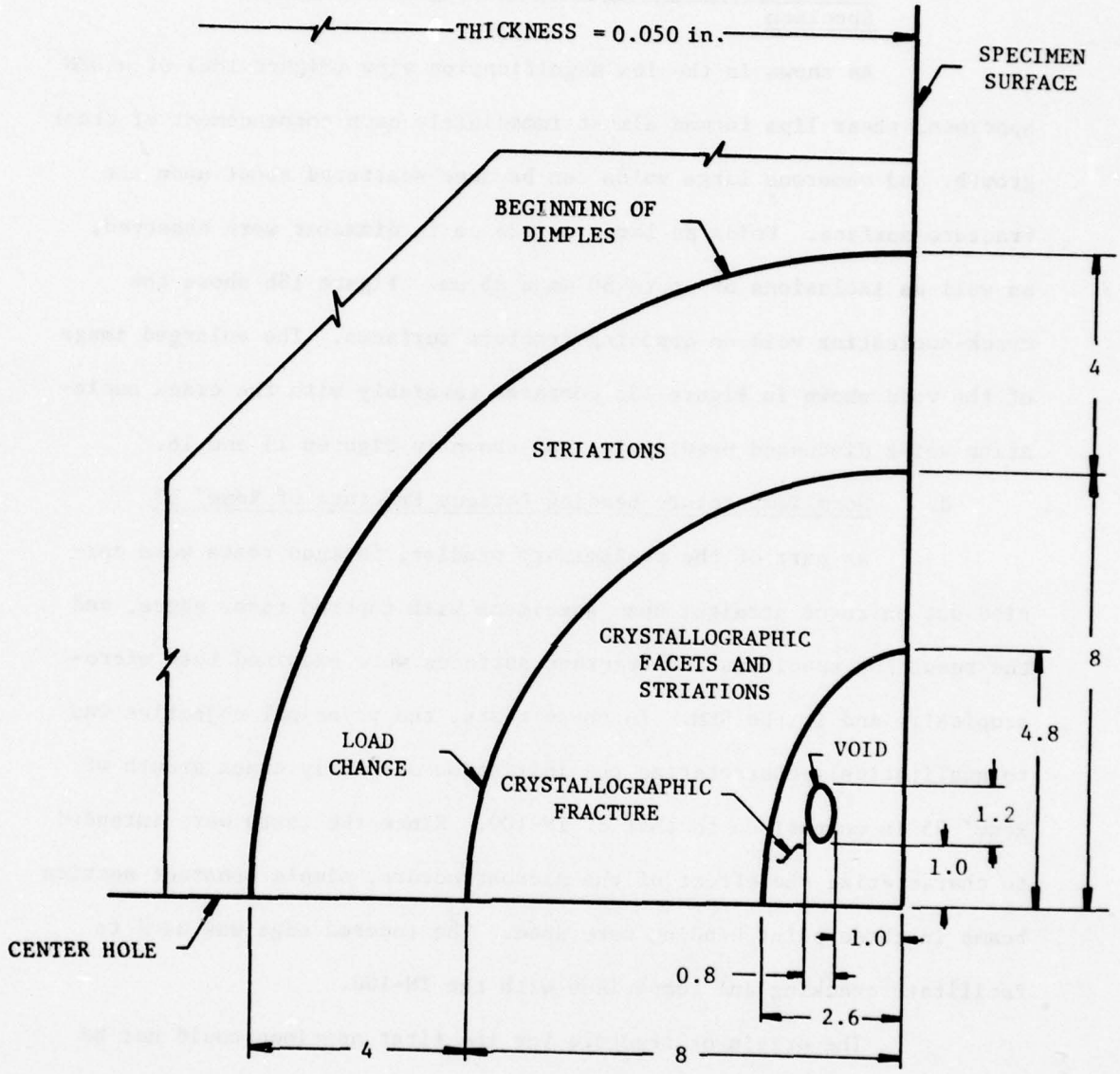

Figure 17. Sketch of Failure Surface of Razor Blade Specimen (Dimensions In in. x 10^{-3})

c. Room Temperature Fatigue Fracture of DEN IN-100 Specimen

As shown in the low magnification view (Figure 18a) of a DEN specimen, shear lips formed almost immediately upon commencement of crack growth, and numerous large voids can be seen scattered about upon the fracture surface. Voids as large as 125 μm in diameter were observed, as well as inclusions of up to 50 μm x 25 μm. Figure 18b shows the crack-nucleating void on opposing fracture surfaces. The enlarged image of the void shown in Figure 18c compares favorably with the crack nucleating voids discussed previously, and shown in Figures 15 and 16.

d. Room Temperature Bending Fatigue Fracture of Rene´ 95

As part of the preliminary studies, fatigue tests were carried out on three straight beam specimens with tapered razor edges, and the resulting specimens and fracture surfaces were examined both microscopically and in the SEM. In these tests, the principal objective was to qualitatively characterize the initiation and early crack growth of Rene´ 95 in comparison to that of IN-100. Since the tests were intended to characterize the effect of the microstructure, simple constant section beams in three point bending were used. The tapered edge was used to facilitate cracking and comparison with the IN-100.

The origin of fracture for the first specimen could not be determined with certainty, although a very small subsurface carbide was detected just below the tip. The general area of the origin was highly faceted and rather featureless.

A cracked carbide lay near the origin of the second fracture, as shown in Figure 19, a head-on view of the taper edge. However, it was impossible to determine the precise role of the carbide in the initiation process, i.e., it may have been cracked a priori, it may

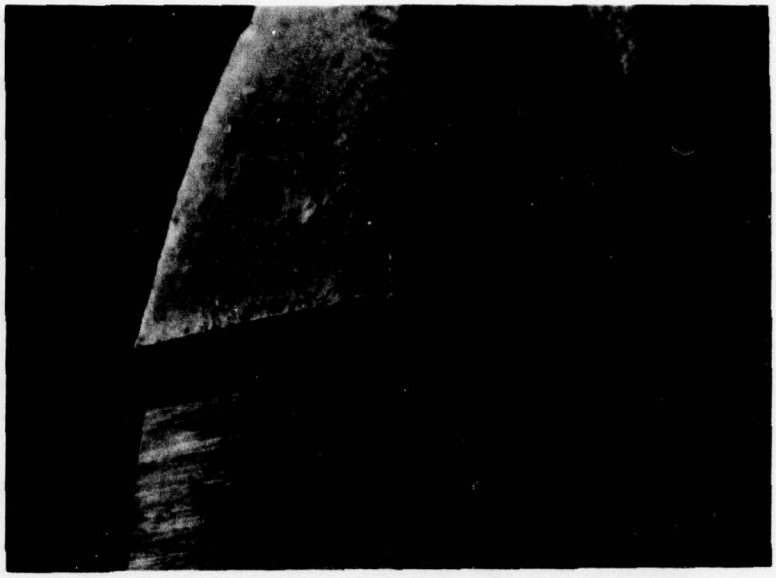

Figure 18a. Macroview of DEN Fatigue Surface. 28X

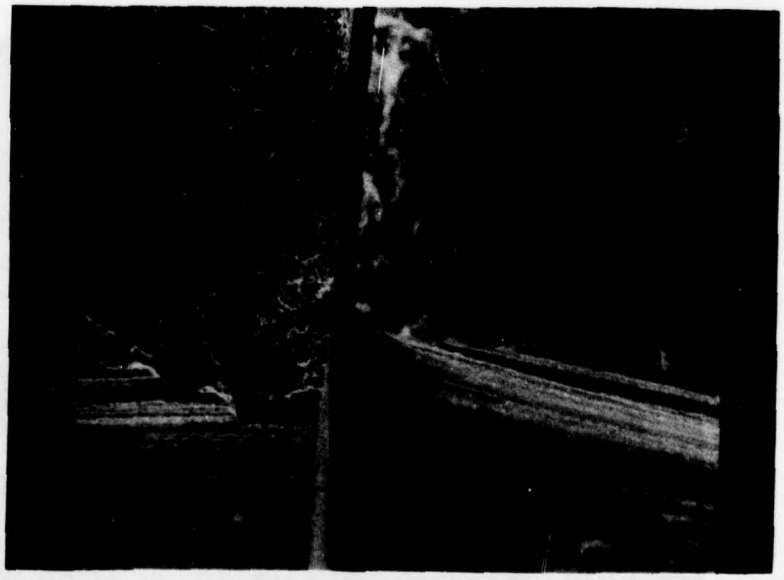

Figure 18b. Void At Origin of Failure in DEN Specimen. 280X

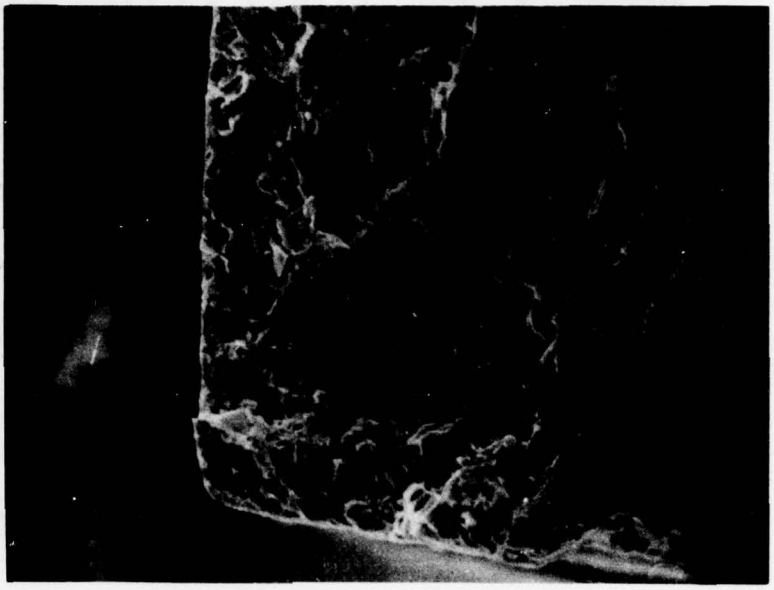

Figure 18c. Closeup of Void. 1120X

Figure 19. Carbide Located At the Taper Edge of Rene' 95 Bending Specimen. 2500X

have failed during cycling, or it may have fractured when the propagating microcrack reached it. Again the fracture surface exhibited the faceted morphology characteristic of Stage I fatigue crack growth.

Finally, one of the Rene´ specimens was fractured by a crack whose initiation was possibly related to a cluster of three inclusions, as shown at the intersection of the specimen edge and crack in Figure 20 (in this case a side view, rather than a fracture surface). However, the extent of this effect is unclear, since the particles seem to be uncracked, and the main crack skirts about them. As in the other two Rene´ specimens, the initiation area is crystallographic and featureless.

e. Room Temperature Fatigue Fracture of Precracked, Reduced-Section IN-100 Razor Blade Specimens

The fractography associated with the room-temperature growth of small microcracks in IN-100 is complex, and quite interesting. Figure 21 shows a low magnification view of such a fracture surface; it is instructive to consider the sequence of events attending its creation.

As described previously, a single edge notched specimen was precracked , and then load shed down to just above the threshold. The specimen was then electro-discharge machined into a reduced-section specimen containing a very short (~75 μm) initial crack (arrows in Figure 21). Cycling was commenced at approximately the same level of stress intensity which was obtained at the cessation of downloading. One of the important fractographic findings was that the fractography was identical on both sides of the line (arrows) separating the two regions, in which a long and a short crack grew at the same low stress intensity. In particular, the microstructure in both regions is predominantly crystallographic, as for example in Figure 22a. As the crack lengthens, there is a gradual transition such that by the time the crack is about 400 μm in

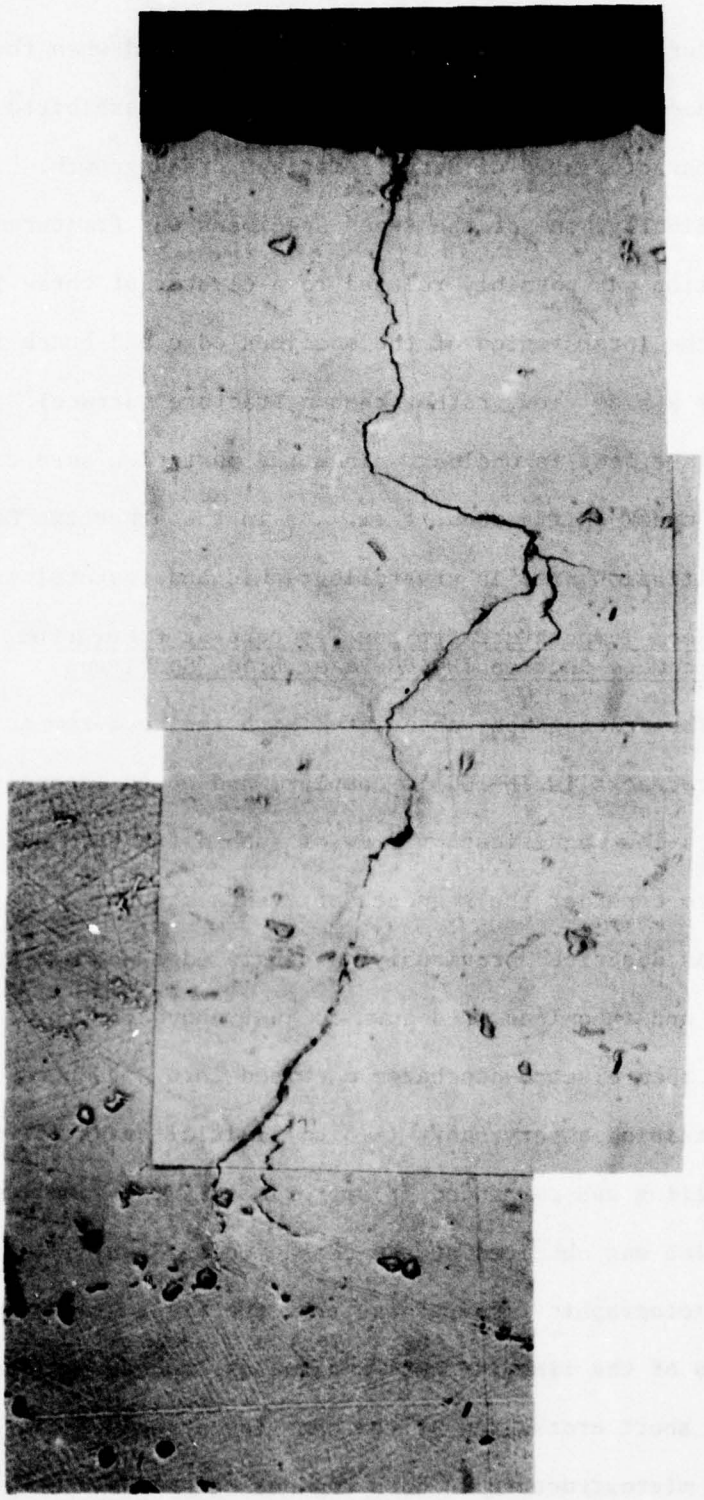

Figure 20. Initial Crack Found In Rene' 95 Bending Specimen #3 After 3.0 * 10^6 Cycles, Left Side. 320X

Figure 21. Fracture Surface of Room Temperature Microcrack Specimen. 100X
Arrows Indicate Initial Crack Length.

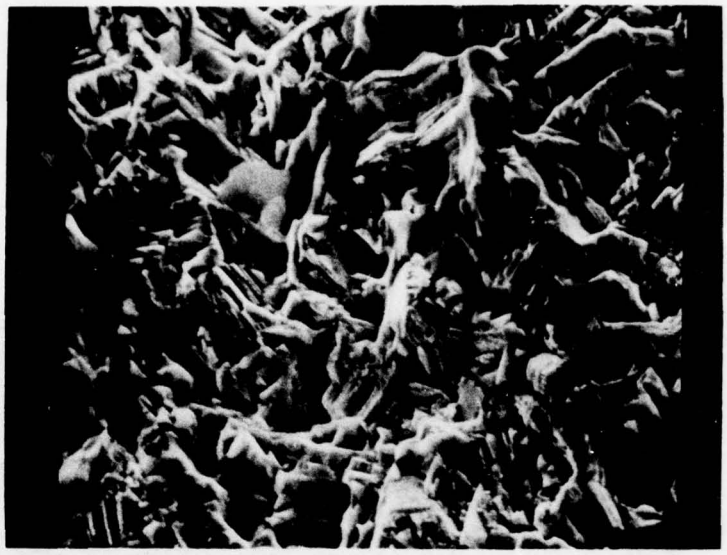

Figure 22a. Crystallographic Fatigue Surface of Room Temperature IN-100. 2500X

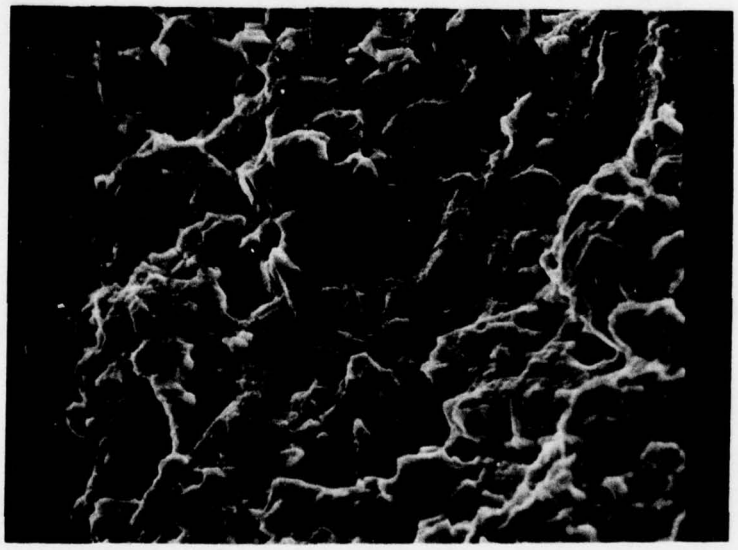

Figure 22b. Striations on IN-100 Fatigue Surface. 3000X

length, the fracture surface (with the exception of the regions along the edge of the specimen) is almost totally covered with striations (Figure 22b).

Some understanding of the nature of this transition can be obtained by etching the fatigue fracture surface in an etch which attacks the γ' phase. As shown in Figure 23a, the early stages of growth are almost entirely transmatrix, since the major portion of the etched surface displays the small cuboid γ' structure common to the matrix. However, the etched structures observed for the striation growth period are dramatically different (Figure 23b), being composed of a great deal of large, blocky γ' superposed on an etched matrix. On this basis, it is clear that during the early stages (low stress intensity) of growth, fatigue cracks in IN-100 tend to avoid the blocky γ' particles; later, during the striation growth regime, they grow right through the blocky γ'.

As pointed out above, the edges of the fracture surface tend to differ from adjoining striated areas. Figure 24a shows the striations which characterize the central portion of the fracture surface for a crack length of about 250 μm. Near the edge, however, the fractography for the same crack length is crystallographic (Figure 24b) rather than striated, and the 10 μm strip nearest the edge is brinelled in many locations. This evidence, and that of Section IV.1.e, indicates that at room temperature, the lack of constraint in the plane stress region facilitates Stage I crack growth. The shear lips formed are visible in Figure 18a.

f. <u>High Temperature Fatigue Fracture of Precracked, Reduced-Section IN-100 Razor Blade Specimens</u>

Two types of high temperature tests were run, as described elsewhere, (1) standard cyclic and (2) one minute dwell cycles. Figure

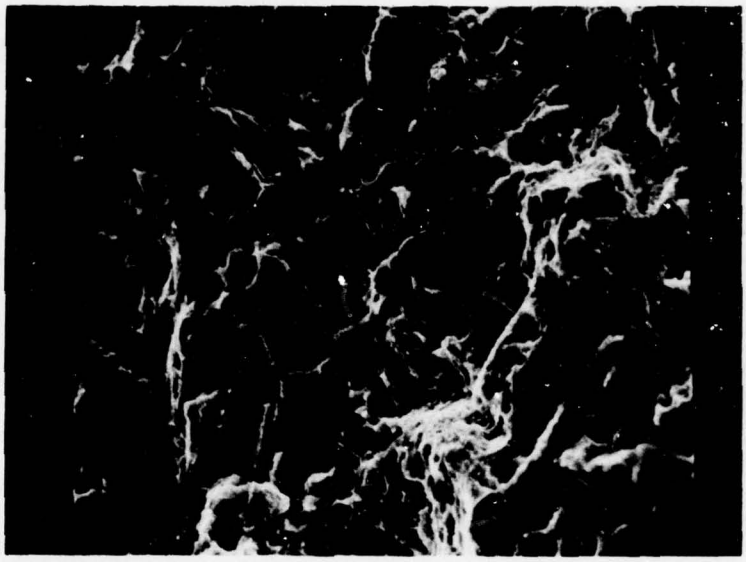

Figure 23a. Etched Crystallographic Fatigue Surface. 3000X

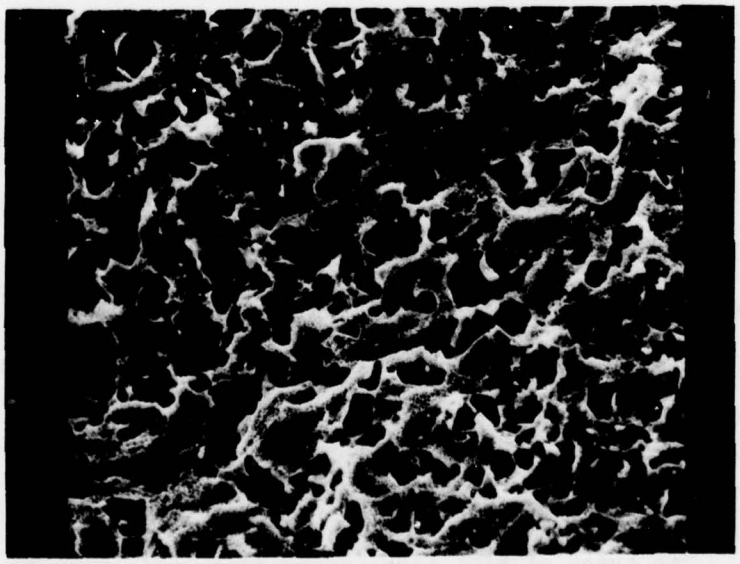

Figure 23b. Etched Striated Fatigue Surface. 3000X

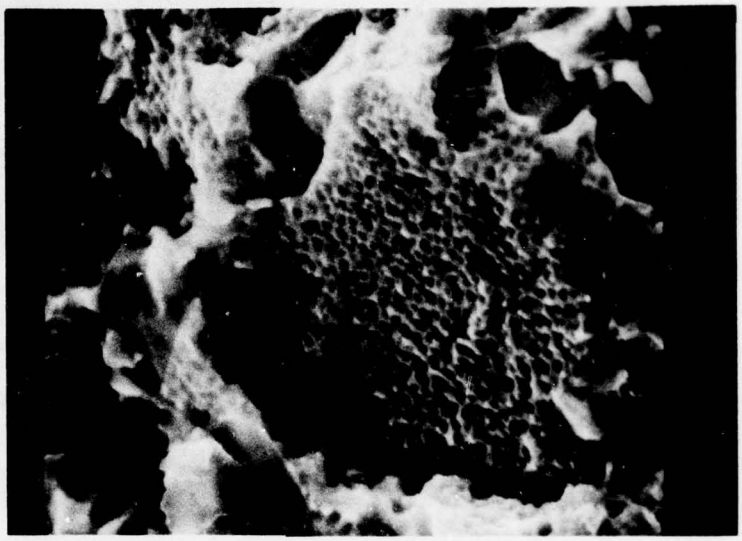

Figure 23c. Higher Magnification View of 23a.
12,000X

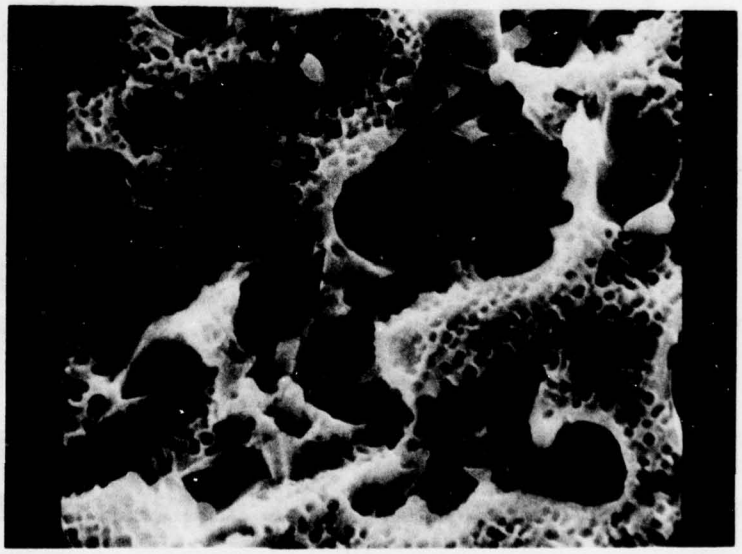

Figure 23d. Higher Magnification View of 23b.
12,000X

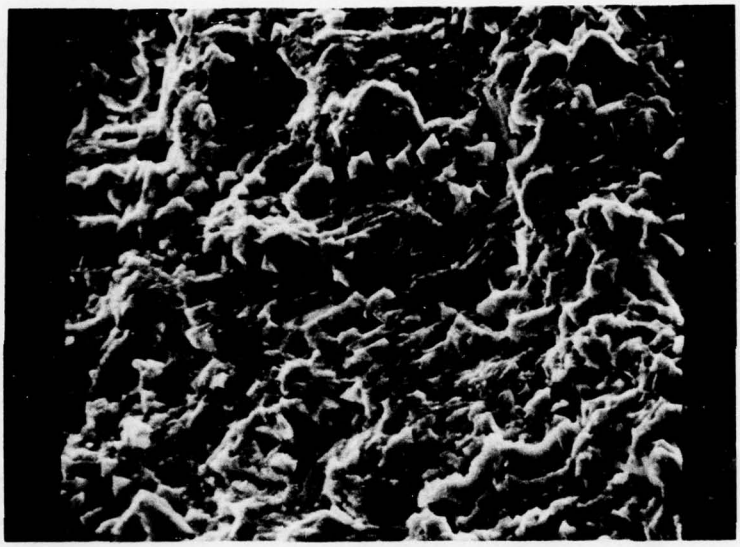

Figure 24a. Striations on Fatigue Surface. 2700X

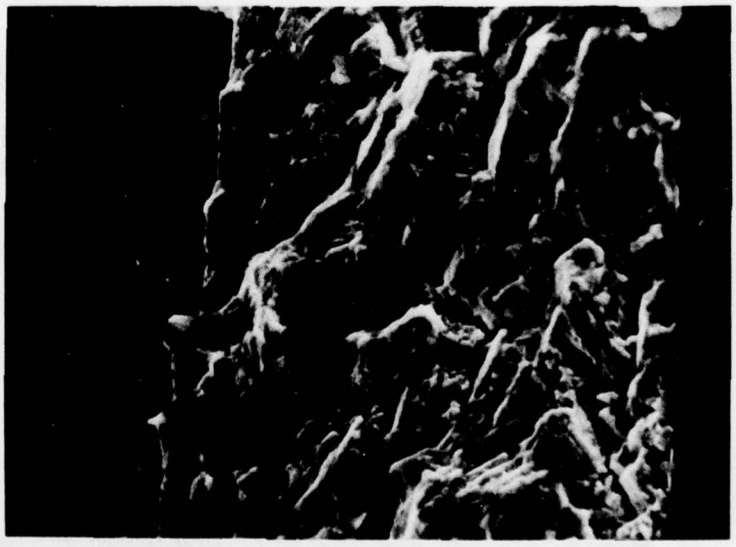

Figure 24b. Crystallographic Region At Specimen Surface. 2700X

25a shows the fracture surface resulting from a standard cyclic test run at 650°C. Two distinct regions can be discerned, as marked by the arrows; the latter correspond to the location of the original precrack. Closer inspection (Figure 25b) shows that precrack region, as before, consists of crystallographic facets. The region formed during high temperature cycling, however, is totally intergranular. The oxide layer formed during the high temperature excursion is insignificant, in terms of its visible effect on surface detail.

No essential difference from this picture was seen for the dwell test at the same temperature (Figures 26-28). Figure 26 shows the fracture at low magnification, with the arrows indicating the extent of the precrack. Crystallographic features found in the precrack region are shown in Figure 27a and in Figure 27b; the latter emphasizes the contrast between the crystallographic mode (right side) and intergranular mode (left side) in the region of the precrack boundary. Away from the specimen edges, the high temperature dwell fractography is totally intergranular (Figure 28a). Near the edges, however, it looks as if the fracture mode may be at least partially transcrystalline, as in the lower portion of Figure 28b; this region of possible mixed-mode growth is only around 25 μm wide.

2. Crack Path and Crack Tip Opening Observations

Optical and scanning electron microscopy were used to study the paths of cracks in IN-100 and Rene´ 95 relative to their respective microstructures. In addition, cracks in IN-100 were grown in a fatigue stage and observed inside the SEM. Again the results for several test conditions are reported.

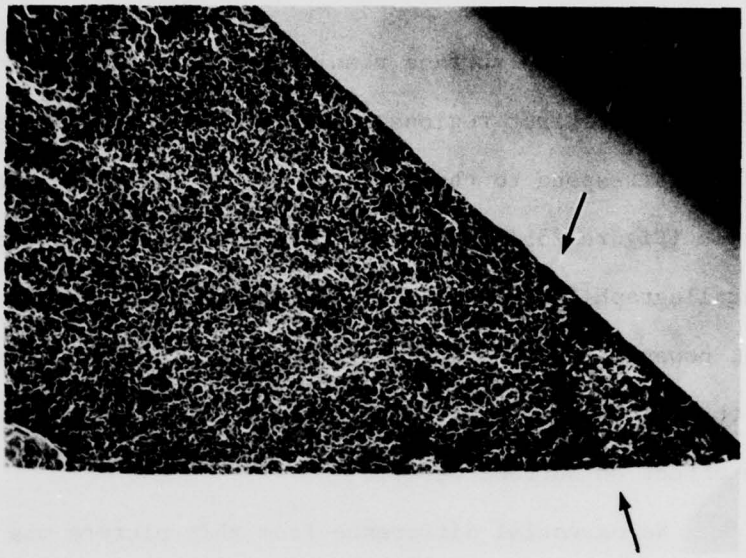

Figure 25a. Fracture Surface of 650°C Cyclic Specimen. 200X
Arrows Indicate Original Precrack Length.

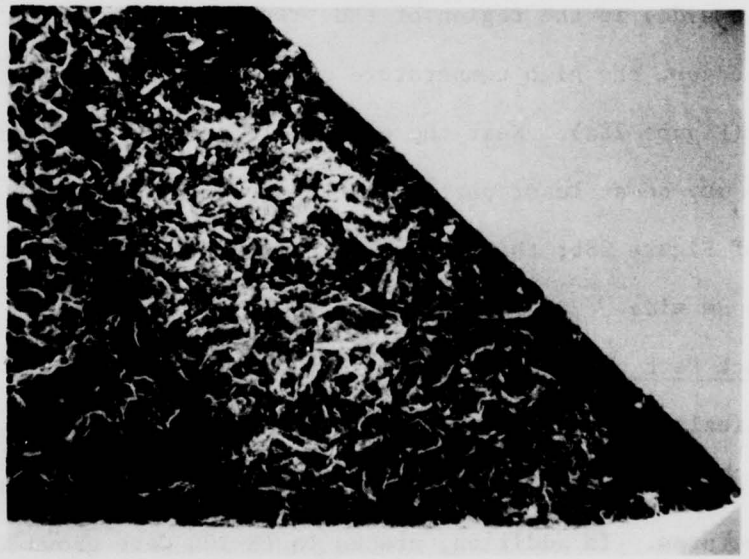

Figure 25b. Comparison of Precrack and 650°C Fatigue Surface. 700X

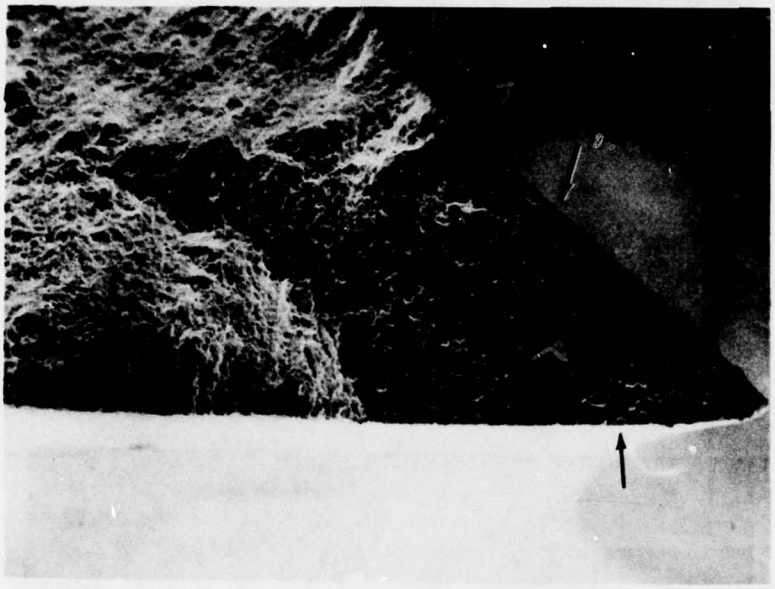

Figure 26. Fracture Surface of 650°C Dwell Specimen. 200X

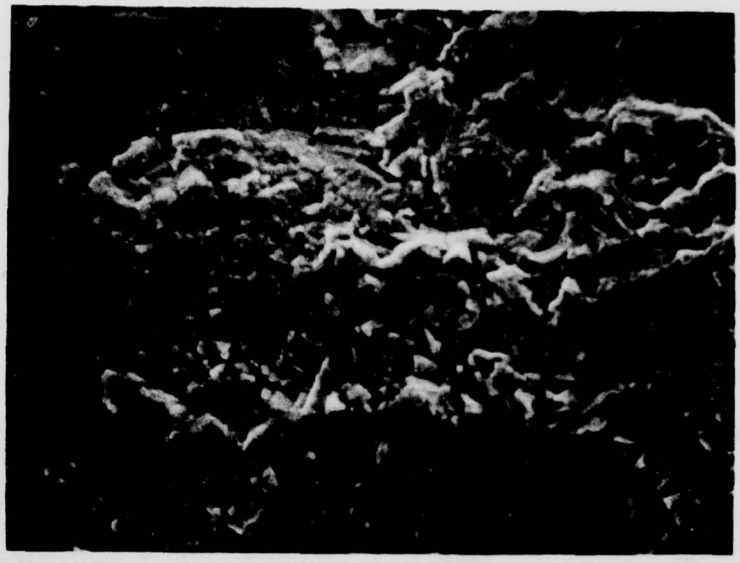

Figure 27a. Crystallographic Surface in Precrack Region. 1500X

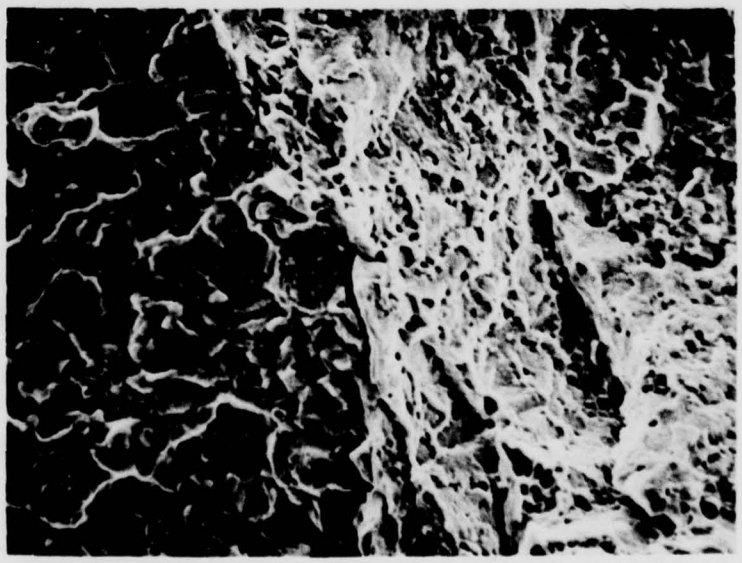

Figure 27b. Comparison of Crystallographic and Intergranular Fatigue Surfaces. 1500X

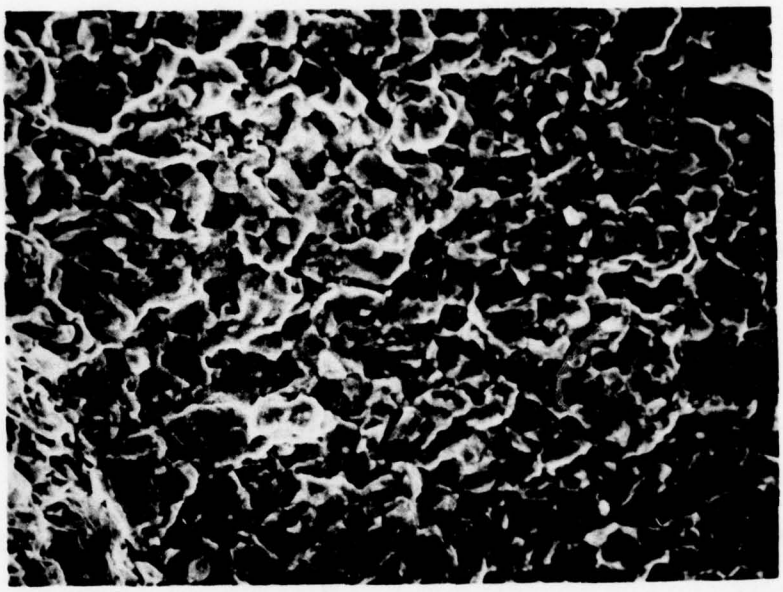

Figure 28a. Fatigue Surface, 650°C Dwell Specimen. 1500X

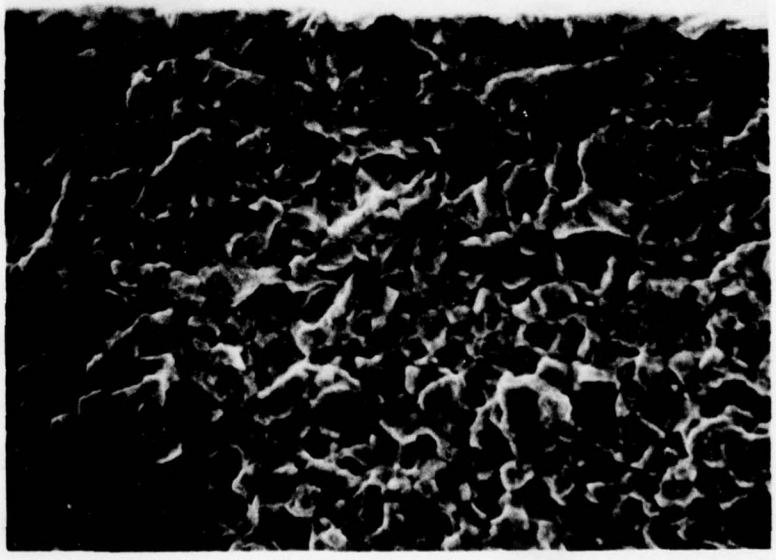

Figure 28b. Fatigue Surface, 650°C Dwell Specimen Near Specimen Edge. 1500X

a. Room Temperature Fatigue Fracture of Rene´ 95

Figure 29 shows the initial crack (250 μm) in one of the Rene´ 95 bending specimens. In Figure 29a, a number of crack branches, and considerable deviation from the plane normal to the applied stress, can be seen. The other side of the specimen (Figure 29b) has a better finish; a number of slip line patterns are visible. The crack does not appear to intersect many carbides, and the three that are encountered are fractured along the interface rather than through the carbide. The crack path seems to have a complex relationship with the surface slip; Figure 30a shows a region in another specimen in which the crack path at times falls within the slip bands, and at other times lies normal to them. The slip packets visible at the top of the photo are approximately 125 μm in length, on the order of the grain size of the material. Figure 30b shows, at higher magnification, the region in which crack growth is normal to the slip bands. Nevertheless, the bulk of the crack growth process seems to involve extension within slip bands, i.e., Stage I growth.

b. Room Temperature Fatigue Fracture of Precracked, Reduced-Section Razor Blade Specimens

Razor blade specimens (Figure 3) containing both "long" (~475 μm) and "short" (~75 μm) microcracks were cycled in the SEM. Crack tip behavior was examined statically, in the loaded/unloaded states, and dynamically, through videotaping of the TV monitor. While some of the results will be demonstrated photographically, others originate from the TV observations, and are simply reported herein. In each case studied, the specimen surface was etched, so that crack tip/microstructure interactions could be determined. In these etched specimens, large blocky γ' particles (0.5 to 1.0 μm), as well as smaller, strengthening γ' cuboids, can be seen.

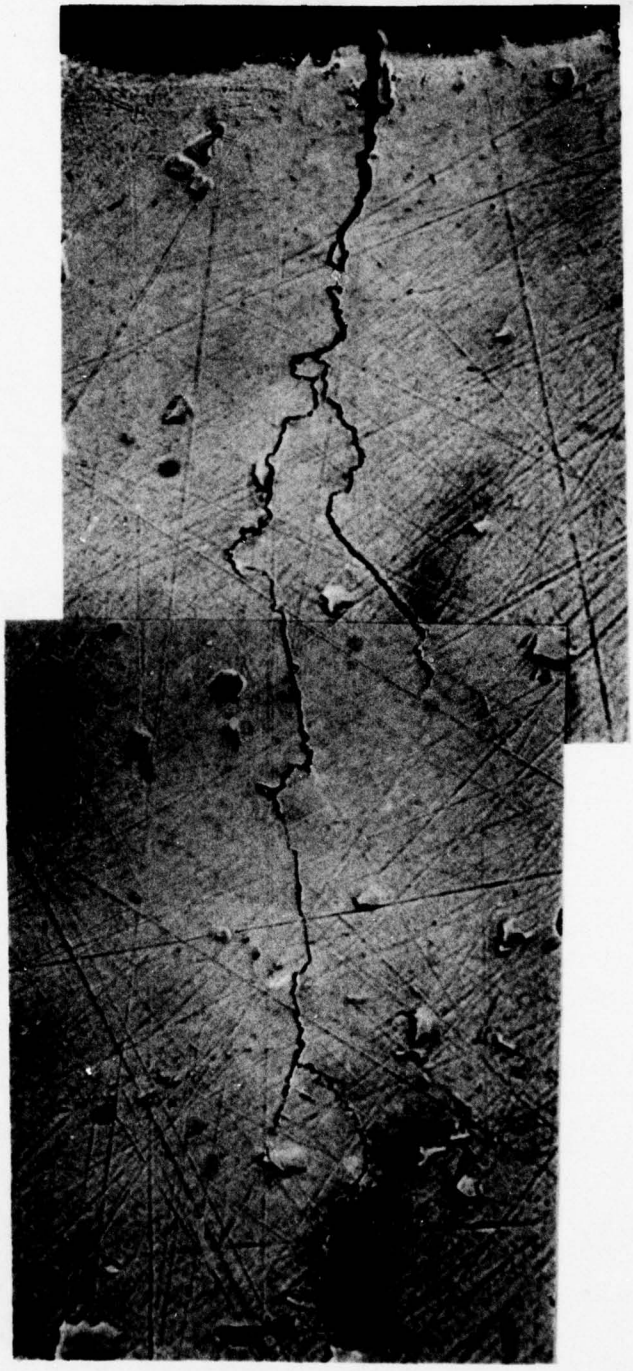

Figure 29a. Initial Crack Found in Rene' 95 Bending Specimen #2 After 1.3 * 10^6 Cycles, Left Side. 645X

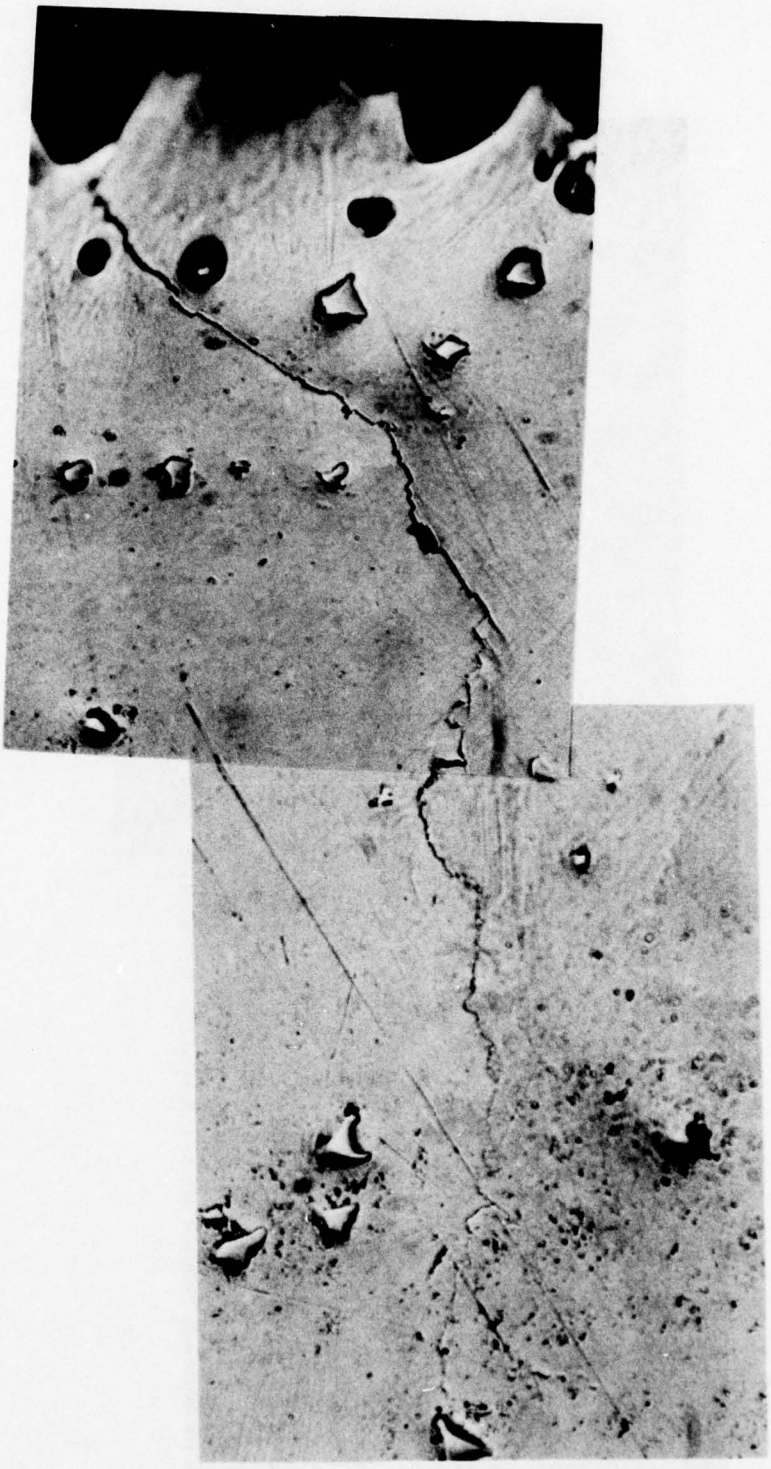

Figure 29b. Rene' 95 Bending Specimen #2, Right Side. 645X

Figure 30a. Rene' 95 Bending Specimen #2, Right Side, Crack Tip and Slip Lines. 320X

Figure 30b. Closeup of Region in Rene' 95 Bending Specimen #2 Showing Fracture Surface and Crack Crossing Slip Region. 2200X

Figure 31a shows an overall view of a short crack prior to cycling. At higher magnification (Figure 31b), it can be seen that during load shedding down to a stress intensity (ΔK) of 14 MPa$\sqrt{m}$, during which period the crack had been very long, the crack tended to pass right through the blocky γ' phase (arrow, Figure 31b). This behavior continued once cycling of the short crack commenced at the same ΔK, as shown in Figure 32, in which the crack has grown approximately 25 μm; arrows indicate microfractured γ' particles.

At higher magnification, the deformation associated with the crack tip can be observed. Figure 33a shows the tip (arrow) of the crack of Figure 32 in the unloaded state, while Figure 33b shows the loaded configuration. In all of these photographs, the stress axis is horizontal, so that it is clear that the crack tip opening includes a significant shear component. Study of such pictures using a new stereoscopic viewing technique, and examination of the TV video sequences, shows clearly that the crack opens by a mixture of Mode I (tensile) and Mode II (shear) crack tip displacement. Moreover, crack propagation is discontinuous, according to the following sequence of events: starting from a sharp crack, blunting of the tip occurs over several cycles; during the blunting, one or more shear bands gradually develop, followed by crack growth within one of the bands.

A typical example of this behavior is seen in Figure 34, which shows the growth of a "long" crack. As it turns out, the blunting/sharpening sequence is essentially identical for both "long" and "short" cracks, in agreement with the fractography results discussed earlier. Considerable microcracking occurs ahead of the crack tip (Figure 35), although the main crack may not link up with each microcrack (Figure 36--

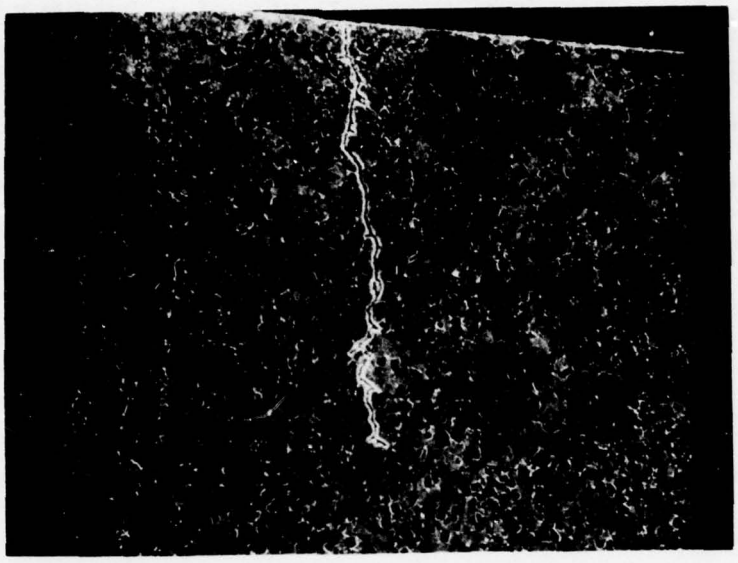

Figure 31a. Fatigue Crack in IN-100 Prior to Cycling in SEM. 600X

Figure 31b. Fatigue Crack Tip Prior to Cycling in SEM. 6000X
Arrows Indicate γ' Which the Crack Has Passed Through.

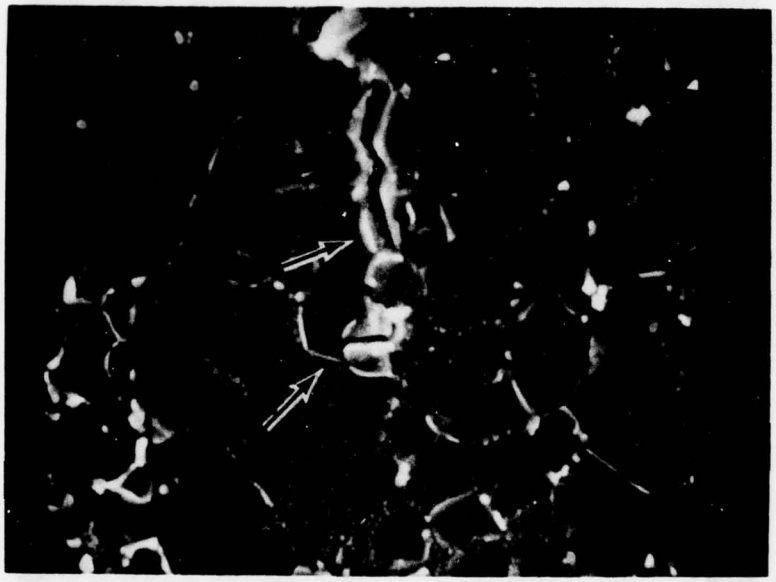

Figure 32. Crack Tip During Cycling
in the SEM. 4000X
Arrows Indicate γ' Particles.

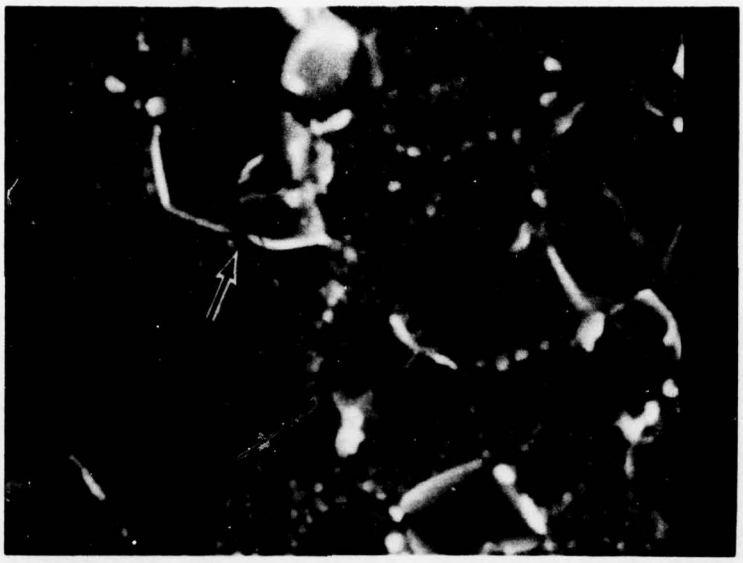

Figure 33a. Closeup of Unloaded Crack Tip.
8000X
Arrow Indicates Crack Tip.

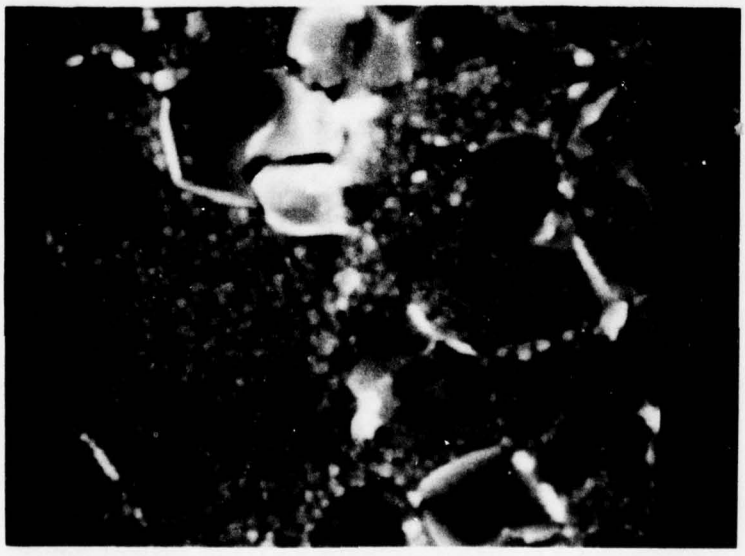

Figure 33b. Closeup of Loaded Crack Tip.
8000X

Figure 34a. Loaded Crack Tip for Crack Length of 0.5 mm. 5000X

Figure 34b. Unloaded Crack Tip. 4000X

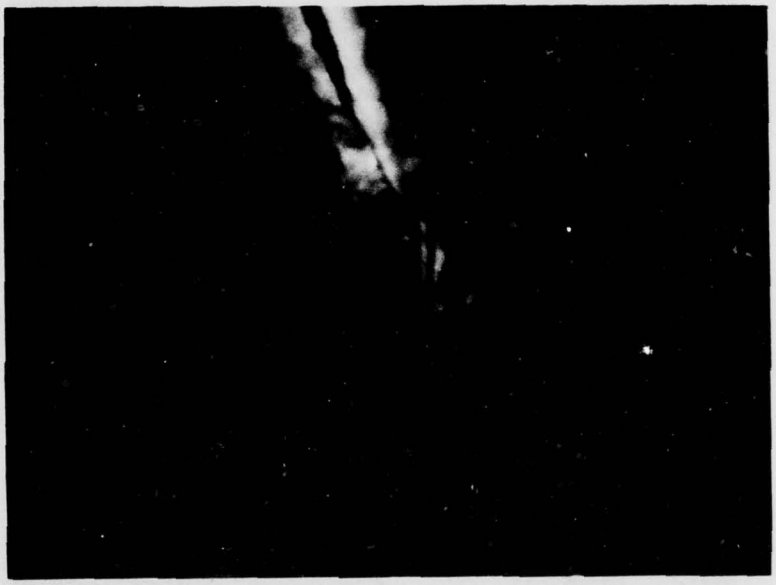

Figure 35. Cracking Ahead of Main Crack.
8000X

Figure 36a. Loaded Crack Tip and Associated Microcrack. 8000X

Figure 36b. Unloaded Crack Tip. 8000X

compare with Figure 35). The sharpness of the cracks, and their crystallographic dependence, is reflected in the low ΔK, crystallographic fractography.

Grain boundaries were observed to play an important role in crack growth dynamics. When a crack (both "long" and "short") encountered a grain boundary, growth was retarded, and CTOD reduced. With continued cycling, plasticity was induced in the blocking grain, CTOD increased, and the crack finally worked the crack tip region into such a state that growth could proceed. When a microcrack was nucleated within the blocking grain, the main crack often simply linked up with it.

SECTION V

DISCUSSION OF RESULTS

In a recent note, Smith [6] has argued that the successful application of continuum based fracture mechanics requires a crack length of approximately 0.25 mm, depending on the material and the specimen geometry. Pearson [7] found for aluminum alloys that when crack length was greater than 0.127 mm, the crack growth rate data agreed with the data obtained from long cracks; for shorter crack lengths, the crack grew faster than would be anticipated from the long crack data. While no theoretical basis for such behavior exists, it is known that for small a/w values for a two dimensional edge flaw, the actual crack tip stresses are higher than are obtained from the asymptotic LEFM result [8,9]. Thus the actual stress intensity value at the crack tip is higher than computed. As the crack lengthens, a/w increases and the stress approaches the LEFM solution. Note that this means that since the stress is decreasing and the crack length is increasing, the stress intensity and therefore the crack growth rate would remain approximately constant for a time, assuming the stress drops off as $1/a^n$, where $n \approx 1/2$. While this provides an explanation for the higher growth rates seen by Pearson and in this experiment, this effect is not restricted to small cracks. Rather it is restricted to cracks that are small relative to the panel width, i.e., $a/w < 0.3$. For the specimens tested, an increase in crack length from 0.075 to 0.25 mm produces only a small change in the stress ahead of the crack. Thus this effect is unlikely to provide the complete answer for the faster growth rate.

Miller [10], in discussing small cracks initiated at notches, has suggested that small cracks will first slow down and then accelerate as they grow. This is due to the notch plastic zone initially dominating the crack tip region, but as the crack grows, its developing plastic zone eventually dominates the notch zone and then the crack accelerates. It was initially thought that this idea could be applied to the taper specimen except that the transition would be due to plane stress-plane strain effects. This, however, now seems unlikely since in the taper specimen, the thickness of the taper is linearly related to the crack length, as is the plastic zone size, since the latter is a function of stress intensity squared [4]. Thus the linear a vs N behavior should continue since whatever the initial condition, i.e., plane stress or strain, this same condition would continue to exist throughout the test.

The results of our experiments indicate that it may not be possible to make generalizations about the applicability of linear elastic fracture mechanics without considering both the material and its mode of fracture. Moreover, the scale of the observation must be taken into account. For example, Figure 37 shows an oblique view of the fracture surface of specimen 3; in this picture, the specimen has been loaded sufficiently to open the crack, but not to cause complete fracture. The highly crystallographic nature of the fracture surface is prominent in this view. Since the crack growth history of this specimen was recorded by photographs, it was possible to locate the crack tip at any time during growth. The plot shows a period of 15,000 cycles during which the crack grew approximately 0.8×10^{-2} mm. During this period, the crack tip showed no growth during two 4,000 cycle periods. This period of arrest corresponds to the time when the crack was attempting

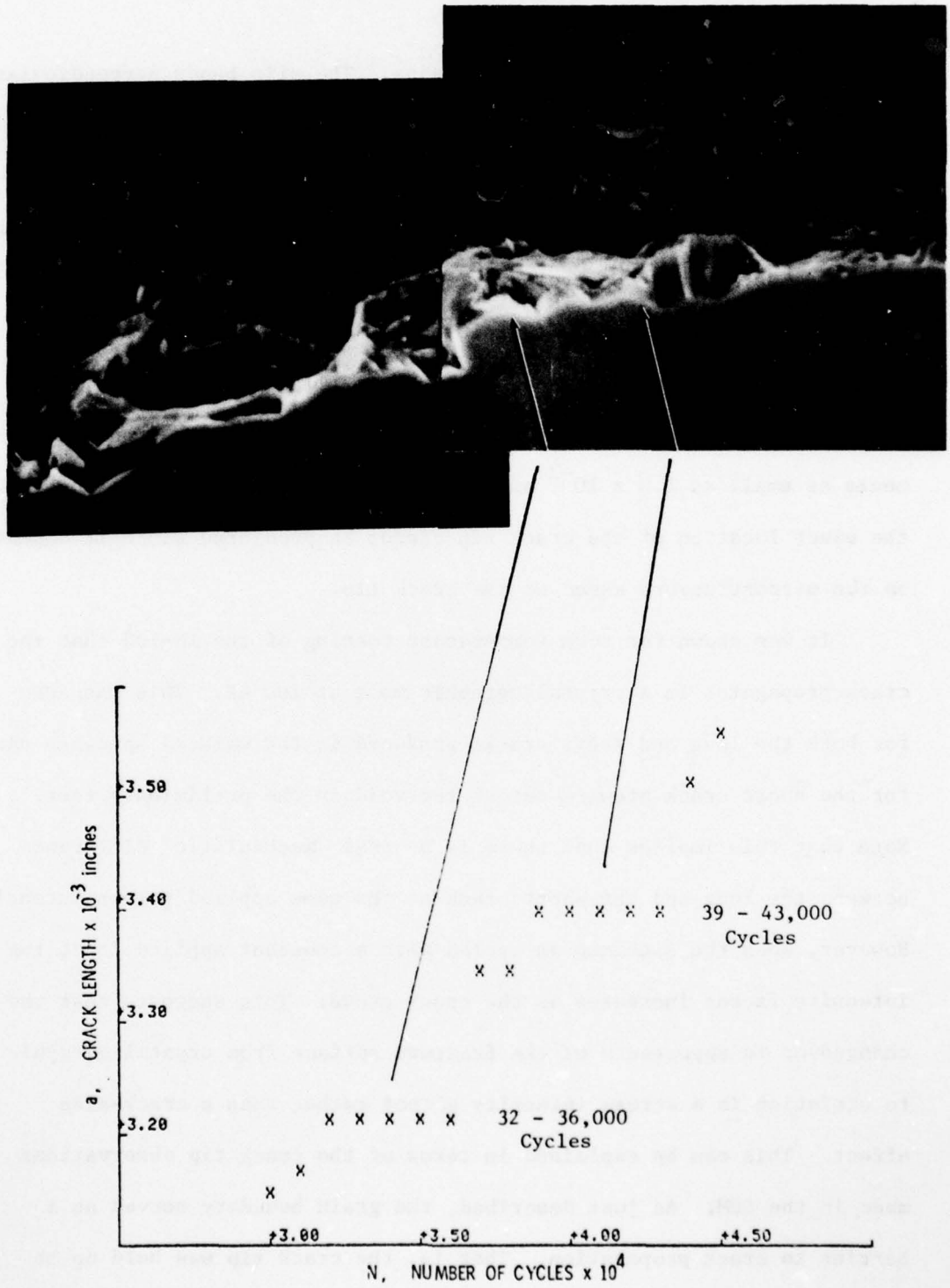

Figure 37. Correspondence Between Fracture Surface and Crack Growth Pattern

to cross two unfavorably oriented grains. The slip bands perpendicular to the path are visible and are denoted by arrows.

From the data shown in the plot, it is clearly impossible to predict a crack growth increment of 0.3×10^{-2} mm on the basis of a continuum based parameter. However, the average growth rate over the 15,000 cycles is 5×10^{-7} mm/cycle (2×10^{-8} in/cycle), which agrees with the rate given in Figure 10 at a ΔK of 12 MPa$\sqrt{m}$ (11 ksi$\sqrt{in.}$). Thus it is possible to make predictions of average crack advance for growth increments as small as 1.0×10^{-2} mm based on continuum parameters; however, the exact location of the crack tip cannot be predicted since it depends on the microstructure ahead of the crack tip.

It was shown for room temperature testing of the IN-100 that the crack propagates in a crystallographic mode at low ΔK. This was seen for both the long and short cracks produced in the waisted specimen and for the short crack growing out of the void in the preliminary test. Note that this implies that there is no real "mechanistic" difference between the long and the short crack at the same applied stress intensity. However, when the specimen is cycled with a constant applied load, the intensity factor increases as the crack grows. This suggests that the changeover in appearance of the fracture surface from crystallographic to striation is a stress intensity effect rather than a crack-size effect. This can be explained in terms of the crack tip observations made in the SEM. As just described, the grain boundary served as a barrier to crack propagation. That is, the crack tip was held up at the boundary until sufficient deformation had taken place to either generate a new crack in the adjoining grain or else accommodate the existing crack tip directly. With the small cracks, the driving force

for this process is small, so that the accommodation takes a longer time and the grain boundaries are more effective in restricting the growth of the crack. In terms of fracture mechanics parameters, at the low ΔK ranges, the cyclic plastic zone is on the order of the grain size or less. Thus the accommodation of the deformation is restricted to a single grain until the crack becomes large enough to generate a cyclic plastic zone size covering several grains. Once several grains are involved, propagation becomes easier since there are more possibilities for planes of easy slip to accommodate the deformation. Assuming that the changeover in appearance is in fact ΔK dependent, then a similar pattern of growth should be observed for long cracks.

Since the slopes of the da/dN versus ΔK relationship are very steep in this regime, the difference in predicted lives using slightly different growth data can be considerable. If a through crack is used with the initial average growth rate observed for specimen 2, for the crack to grow from 0.075 mm to 0.25, requires

$$\Delta N = \frac{\Delta a}{2.3 \times 10^{-6} \text{ mm/cycle}} = 7.6 \times 10^{4} \text{ cycles}$$

On the other hand, if we follow the usual data reduction process and fit an exponential curve to the data, we obtain a growth rate curve of

$$\frac{da}{dN} = 4.9 \times 10^{-19} \ \Delta K^{2.3} \quad \text{(m/cycle)}$$

Integrating this over the same range of parameters yields a life of

$$\Delta N = 4.4 \times 10^{11} \text{ cycles}$$

This shows that the higher than expected growth rate can have a very

large effect on the predicted life of a specimen. Of course, since the data being fitted exist over such a narrow range, the coefficients can undergo a large change with only a small change in the data. However, the relatively short lives seen in the present experiments suggest that the small fatigue cracks may, at least in a PM nickel base superalloy at room temperature, be growing faster than would be expected. It should be emphasized that this statement needs to be examined critically since crack initiation and near threshold behavior is intimately linked to the voids. Thus the question of the behavior of small fatigue cracks that have initiated at a void has not been resolved.

The fact that similar low ΔK behavior was not observed at high temperature is apparently due to the change in crack propagation mode. Since the yield stress is only slightly lower at 650°C, the deformation fields should be similar at the two temperatures. The completely intergranular fracture surface at 650°C means the deformation is being accommodated at the grain boundaries. Hence the boundaries themselves cannot act in the role of barriers as they do at room temperature. The large number of grain boundaries in the PM material apparently facilitates the accommodation of the deformation and therefore results in a much higher crack propagation rate. The presence of striations on the Pratt and Whitney LCF specimen, but not in our tests, is puzzling, but the LCF specimen was tested at 538°C instead of 650°C. This temperature differential could well be the reason for the difference in fracture mode.

It was noted that the crack growth rate observed for the small crack specimens subjected to sinusoidal loading was comparable to that measured using conventional specimens with large cracks. The dwell specimen, however, had a crack growth rate somewhat slower than the data

from the conventional specimen. As previously discussed, there exist some differences in experimental technique that could account for the difference. However, a comparison of the elevated temperature fracture surfaces, Figures 25 - 28, shows that while the elevated fracture surfaces are intergranular, Figure 26 suggests that there may have been some loss in through thickness constraint in the hold time specimen. The increased time at maximum load in the dwell specimen could be producing additional plastic strain at the surfaces of the specimen through local relaxation of the stress. In general, the high constraint plane strain regions tend to promote creep crack growth, so the slower crack growth observed in the present tests could be a time dependent thickness effect.

It appears that the room temperature transition from crystallographic to striated growth is accompanied by a change in the relationship between the crack plane and the constituent phases. During early stages of growth, the crack is able to grow through the small γ' cuboids, but avoids the large block gamma primes. At a higher ΔK, the crack finally is able to begin growing through the latter, producing a totally striated surface. This reflects the increasing cyclic plastic zone size as discussed in connection with the grain boundaries. For small plastic zones, the large precipitates are not enclosed in the fracture regime, but as the zone size increases, the large gamma primes are included in the zone and can be fractured directly.

The crystallographic morphology characteristic of the edge of the fracture surface following the general transition to striated growth may be caused by the presence of the surface as a stress field modifier, i.e., crystallographic growth may be characteristic of plane stress. If so, one must be concerned with whether surface observations are actually

representative of the subsurface state of affairs. This will not affect many of the room temperature observations since crystallographic growth also took place in regions that were clearly plane strain. One must use care in interpreting the observations when the subsurface region is forming striations.

For the cyclic stress intensities used in this study, the crack tip plastic zone was calculated to be a small fraction of the (local) specimen thickness. Thus, the observed mixed mode crack opening is believed to be typical of the entire thickness. In the same vein, the crack plane is not perpendicular to the load axis on a microscopic scale, but rather is made up of tiny, inclined shear planes, indicating the importance of mixed mode crack growth over the entire thickness. In fact, one of the key results of the SEM observations is the appreciation of the very complex deformation field that exists around the crack tip; detailed determination of such fields was not part of this program.

As was discussed in connection with the dwell specimen at 650°C, there may have been a thickness effect for this one specimen. This, of course, is a time dependent effect and does not affect the SEM observations or the lower temperature observations.

SECTION VI

CONCLUSIONS

The present study of the applicability of linear elastic fracture mechanics to very small fatigue cracks in the PM superalloy IN-100 has reached the following conclusions.

1. At room temperature, there is no difference in the mechanism of crack growth for long and short cracks at the same range of stress intensity factor. The growth is entirely crystallographic at low ΔK.
2. As the crack lengthens, the room temperature growth mechanism changes to striation formation. This effect appears to be due to the increasing stress intensity factor.
3. At room temperature, the small cracks appear to have higher growth rates than would be predicted on the basis of large crack data. This behavior is observed only at low ΔK values. At ΔK values above 16 MPa$\sqrt{m}$, the small and large crack growth data showed good agreement.
4. At 650°C, no difference was found between small and large crack growth rates for continuous cycling. The mechanism of crack growth was intergranular.
5. At 650°C, the one minute dwell time growth rate was approximately five times slower for the small crack than the large crack. This may be attributed to increased time dependent plastic deformation at the surface slowing the crack.
6. Real time observation of growing fatigue cracks in the SEM has shown that the interaction between the crack tip and the

microstructure is very complex. The grain boundaries do present an effective barrier to crack growth at room temperature.

7. Examination of a number of fatigue specimens showed that fatigue crack initiation in this alloy is often associated with a void.

8. Interferometric measurement of plastic zone size has been shown to be an accurate technique for determining stress intensity factors.

9. A new etching technique was developed that satisfactorily revealed the alloy microstructure without severe attack to the material.

SECTION VII

REFERENCES

1. D. L. Davidson and A. Nagy, "A Low Frequency Cyclic Loading Stage for the SEM," J. Phys. E: Sci. Instrum., 11, 1978, p 207.
2. G. G. Annis, Jr., R. M. Wallace, and D. L. Sims, AFML-TR-76-176, November 1976.
3. A. F. Liu, Engng. Frac. Mech., 4, 1972, p 176.
4. G. P. Sheldon, T. S. Cook, J. W. Jones, and J. Lankford, "Some Observations on Small Fatigue Cracks in a Superalloy," to be submitted to Int. J. of Fracture.
5. A. E. Gemma, unpublished data.
6. R. A. Smith, Int. J. of Fracture, 13, 1977, p 717.
7. S. Pearson, Engng. Frac. Mech., 7, 2, 1975, p 235.
8. A. Talug and K. Reifsnyder, Cyclic Stress-Strain and Plastic Deformation Aspects of Fatigue Crack Growth, ASTM STP 637, 1977, p 81.
9. D. Tracey, unpublished research.
10. R. A. Smith and K. J. Miller, Int. J. Mech. Sci., 20, 1978, p 201.

AD-A065 180 SOUTHWEST RESEARCH INST SAN ANTONIO TEX F/G 11/6
RESEARCH ON GROWTH OF MICROCRACKS IN NICKEL-BASE SUPERALLOYS.(U)
SEP 78 T S COOK, J LANKFORD, G P SHELDON F33615-76-C-5242
UNCLASSIFIED SWRI-02-4601 AFML-TR-78-133 NL

2 OF 2
ADA
065180

END
DATE
FILMED
4-79
DDC

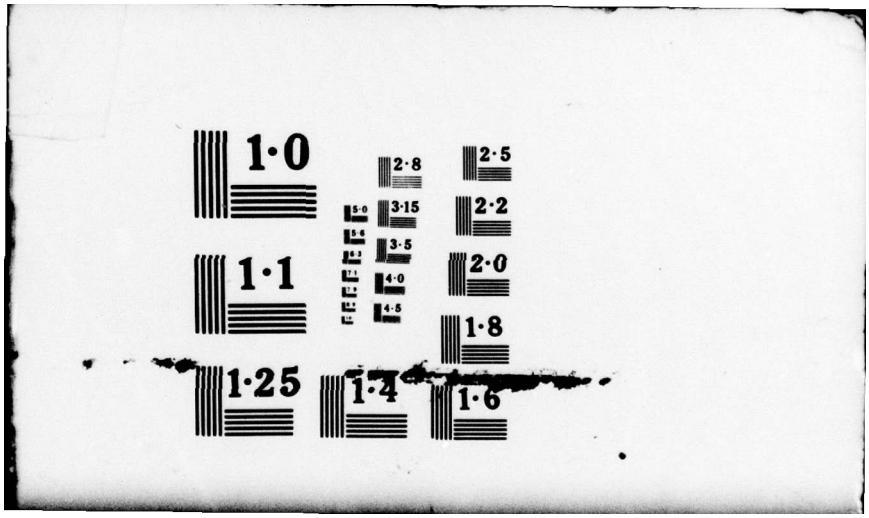
1·0
1·1
1·25
1·4
1·6
1·8
2·0
2·2
2·5
2·8
3·15
3·5
4·0
4·5

APPENDIX

ESTIMATION OF STRESS INTENSITY FACTORS BASED ON INTERFEROMETRIC MEASUREMENTS OF CRACK TIP PLASTIC ZONE SIZE

In general, the extent of plastic deformation surrounding a propagating fatigue crack can be expressed in terms of the maximum applied stress intensity and the material's yield strength as:

$$r_y = \beta \left(\frac{K_{max}}{\sigma_y} \right)^2 \tag{1A}$$

where β is assumed to depend only on the material. In this discussion r_y is the height of the plastic zone as shown in Figure 1A. It should, therefore, be possible to experimentally determine K_{max} as a function of crack length and applied stress simply by the determination of the constant β and the measurement of the plastic zone height r_y. For the small crack in the specimen configuration shown in Figure 3, the stress intensity factor can be expressed as:

$$K = \alpha\sigma\sqrt{\pi a} \tag{2A}$$

where α is a geometric correction factor which may depend on crack length. Substitution of (2A) into (1A) yields:

$$r_y = \beta \left(\frac{\alpha\sigma}{\sigma_y} \right)^2 \pi a \tag{3A}$$

For constant load and α independent of crack length, (3A) indicates that the width of the plastic zone varies linearly with crack length. Determination of β requires the measurement of r_y in a specimen of known stress intensity calibration.

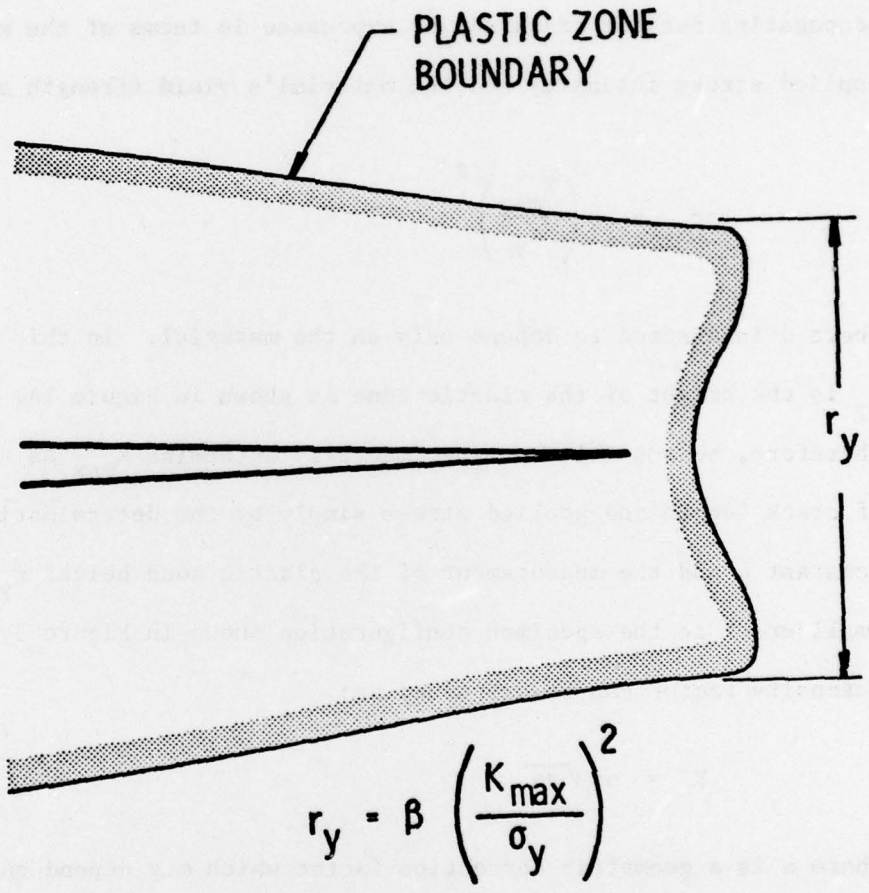

Figure 1A. Geometry of Crack Tip Plastic Zone

In order to check the stress intensity relationship for the specimen configuration in question, r_y was determined by measuring the residual out-of-plane displacements along the crack line at the specimen surface. A specimen containing a 5.56 mm (0.022 in.) crack was examined using a Zeiss Interference Microscope with thallium illumination. The intereference fringe density obtained with the nominally flat specimen surface was increased by introducing an appropriate tilt angle between the specimen and the optical axis of the microscope. In a method similar to that for interferometrically determining the width and depth of a groove in a flat surface, the residual deformation field surrounding the crack was determined. The resulting fringe pattern and the residual deformation field deduced are shown in Figures 2A and 3A. The height of the residual deformation field was assumed to be equivalent to the surface plastic zone height and, as expected from (3A), was found to vary linearly with crack length as:

$$r_y = 2.007 + 18.03\ a \qquad (4A)$$

where the dimensions are millimeters. The finite zone width at a zero crack length resulted from the method of obtaining specimens with small initial flaws as described above.

Similar measurements were made on a modified compact tension specimen of IN-100. For this specimen geometry:

$$K = \frac{P\sqrt{a}\ Y}{BW} \qquad (5A)$$

where:

$$Y = 30.96 - 195.8(a/W) + 730.6(a/W)^2 - 1186.3(a/W)^3 + 754.6(a/W)^4$$

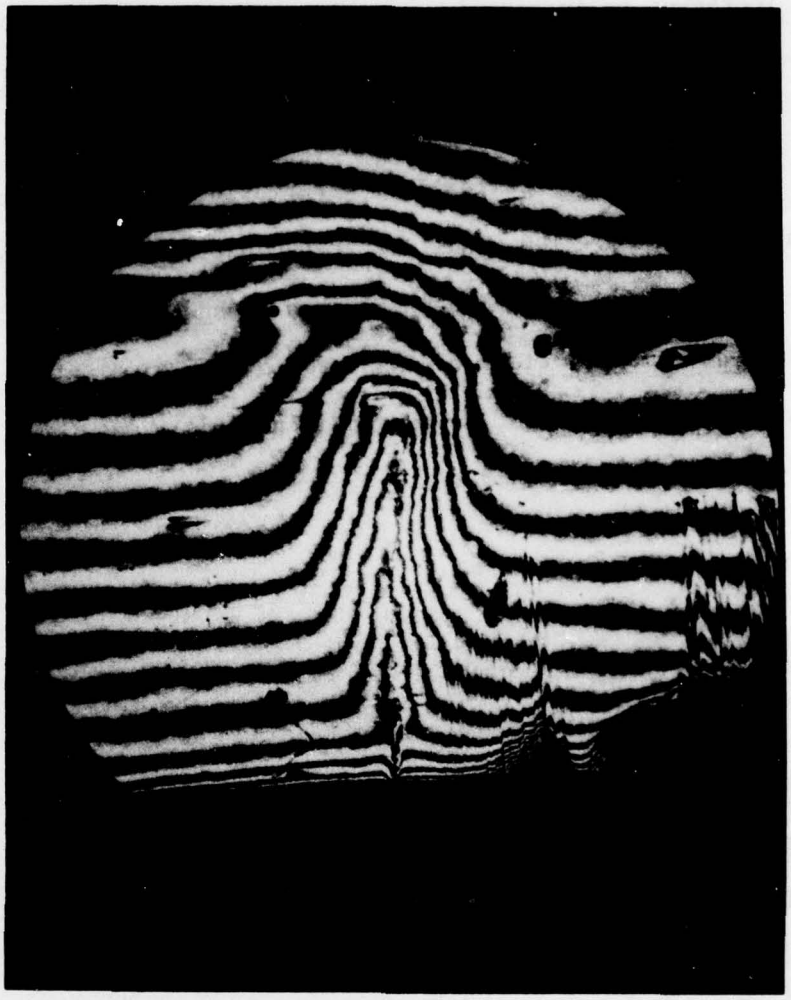

Figure 2A. Interference Micrograph of 0.56 mm Crack in IN-100

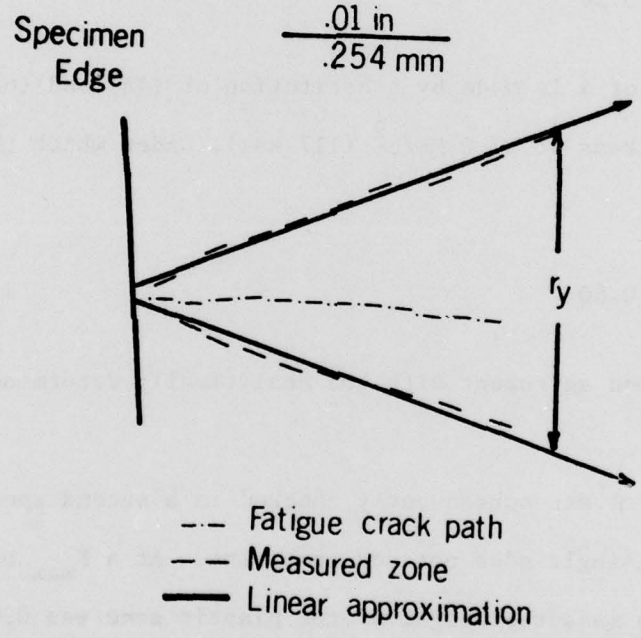

Figure 3A. Deformation Field Carefully Traced From Figure 2A to Indicate Approximations Made

and B = 12.7 mm (0.5 in.), W = 63.5 mm (2.5 in.) and a_n = 15.2 mm (0.6 in.) are the thickness, width and notch length, respectively. P is the applied load. A fatigue crack was grown at a constant K_{max} of 38.5 $MN/m^{3/2}$ (35 $ksi\sqrt{in.}$) by load shedding with K_{min}/K_{max} = 0.1. This produced a plastic zone height of 0.71 mm (0.028 in.) which was independent of crack length. Substituting into (1A) yields:

$$\beta = 0.56 \qquad (6A)$$

The determination of α is made by substitution of (4A) and (6A) into (3A). For the applied stress of 17.0 MN/m^2 (117 ksi), under which the small crack was grown:

$$\alpha = 0.80$$

This is in very good agreement with the analytically determined value of α = 0.82.

The value of β was subsequently checked in a second specimen, one of the precracked single edge notched specimens. At a K_{max} of 9.6 $MN/m^{3/2}$ (8.7 $ksi\sqrt{in.}$), the measured height of the plastic zone was 0.04 mm (1.6 x 10^{-3} in.). Using relation (1A), we obtain

$$\beta = 0.52$$

The latter figure was obtained by means of a multi-beam interference attachment for a standard metallurgical microscope. The fact that the result was obtained by different experimenters, using a different interferometric setup, and with a different specimen design, yet agrees so well with (6A), serves to give additional confidence in the value.

ACKNOWLEDGEMENT

The laser interferometric work described in the appendix was performed by Dr. Wayne Jones at the Air Force Materials Laboratory under the sponsorship of the National Research Council. His assistance in this program is gratefully acknowledged.

*U.S.Government Printing Office: 1979 — 657-002/373